ACS Macro Letters

pubs.acs.org/macroletters Letter

Resolving the Mechanisms of Soy Glycinin Self-Coacervation and Hollow-Condensate Formation

Nannan Chen,* Ziliang Zhao, Yong Wang, and Rumiana Dimova*

Cite This: ACS Macro Lett. 2020, 9, 1844−1852 Read Online

ACCESS | Metrics & More | Article Recommendations | Supporting Information

ABSTRACT: Self-coacervation of animal-derived proteins has been extensively investigated while that of plant proteins remains largely unexplored. Here, we study the process of soy glycinin self-coacervation and transformation into hollow condensates. The protein hexameric structure composed of hydrophilic and hydrophobic polypeptides is crucial for coacervation. The process is driven by charge screening of the intrinsically disordered region of acidic polypeptides, allowing for weak hydrophobic interactions between exposed hydrophobic polypeptides. We find that the coacervate surface exhibits order, which stabilizes the coacervate shape during hollow-condensate formation. The latter process occurs via nucleation and growth of protein-poor phase in the coacervate interior, during which another ordered layer at the inner surface is formed. Aging enhances the stability of both coacervates and hollow condensates. Understanding plant protein coacervation holds promises for fabricating novel functional materials.

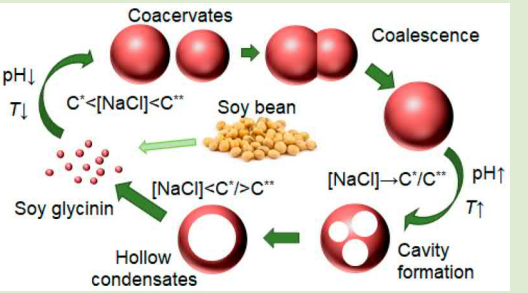

Protein coacervation or liquid−liquid phase separation in protein solutions is characterized by the formation of liquid-like protein-rich microdroplets (coacervates or condensates). Upon coalescence, they yield a macroscopically monophasic biomacromolecular fluid of highly concentrated protein phase.[1] Coacervation can occur spontaneously upon changing the environmental conditions, a process known as simple coacervation or self-coacervation,[2] or via interactions with another oppositely charged protein specie, also known as complex coacervation.[3] Protein coacervation represents a crucial route for the assembly of cellular organelles[4,5] and, at the same time, offers a facile approach toward the fabrication of biomaterials such as fibers,[6] bioadhesives,[7] and bioactive compound carriers.[8] In recent years, much interest has been dedicated to human intracellular condensates originating from intrinsically disordered proteins as well as coacervates that derive from animal extracellular matrix proteins.[4−7] Far less studies have focused on plant protein coacervation.

Compared to animal proteins, plant, and in particular soy proteins are widely abundant and economical, which makes them ideal materials for the scale-up processing in industry. Soy glycinin is one of the major storage proteins in the soybean seed. It is commonly used as an emulsion stabilizer for improving the texture of food products via modulating the structure of protein gels and for producing bioadhesives.[9−11] Recently, soy glycinin was found to undergo self-coacervation in aqueous solutions upon the addition of salt, a process exemplified by the formation of spherical condensates in the micrometer range.[12] Interestingly, upon a temperature increase, the coacervates transform into stable hollow microcapsule-like condensates (also referred to as vacuolated structures or a vesicle-like condensate phase).[12,13] This process represents a simple and very energy-efficient route for microencapsulation of active compounds for controlled release, protection against environmental factors, or masking of an unpleasant odor or taste.[14−16] By forming a protein layer on oil droplets, protein self-coacervation can be employed for the encapsulation of hydrophobic compounds,[17] which represent a much simpler approach compared to traditional methods based on complex coacervation with another polymer, usually polysaccharide.[14] Hollow protein microcapsules formed via coacervation can encapsulate and control the release of hydrophilic compounds by modulating the permeability of the protein shell.[13,18] This is advantageous compared to more popular methods for microcapsule production such as the template-based layer-by-layer method,[19] which involves a tedious and time-consuming fabrication process and is associated with waste of materials.

Despite the above-mentioned advantages and potential applications, the mechanism of soy glycinin self-coacervation and the cavitation of the condensates is not yet understood. Remarkably, the formation of hollow condensates upon self-coacervation has not yet been reported for animal proteins, while it seems a common phenomenon for the plant seed 11S

Received: October 1, 2020
Accepted: November 30, 2020

https://dx.doi.org/10.1021/acsmacrolett.0c00709
ACS Macro Lett. 2020, 9, 1844−1852

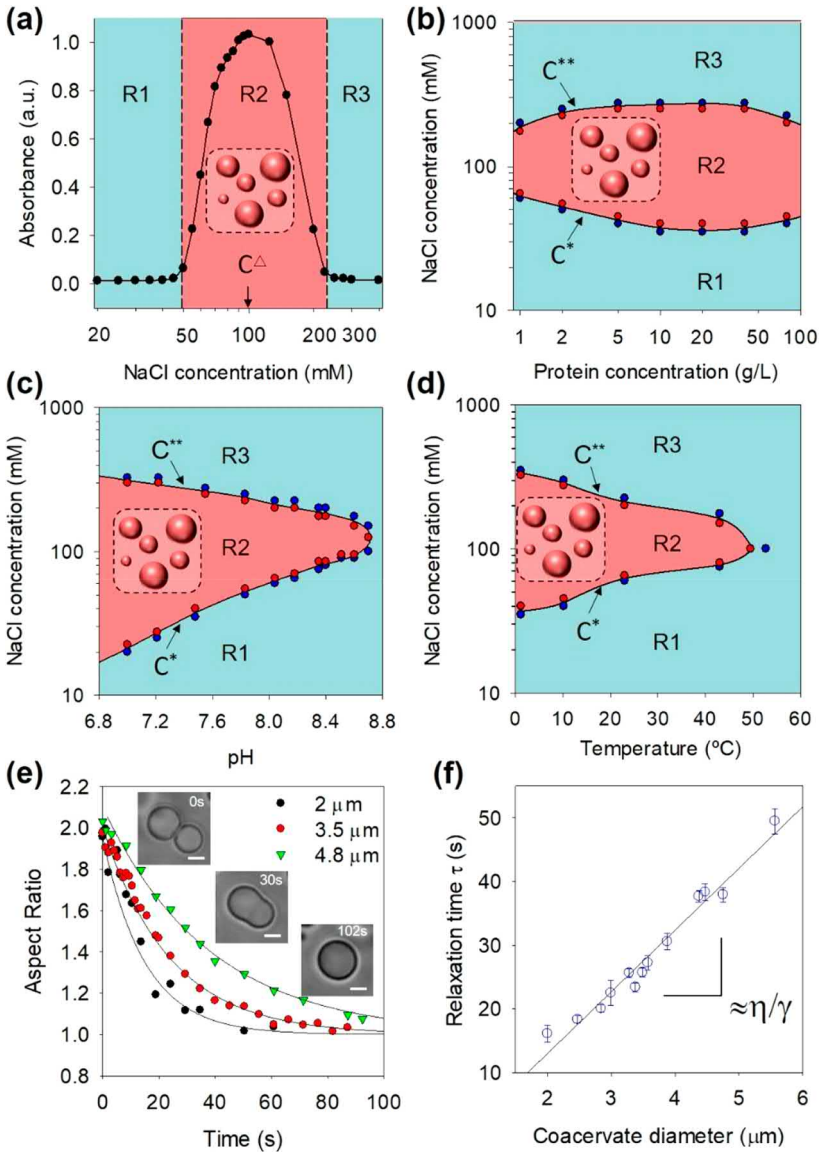

Figure 1. Phase diagrams of soy glycinin coacervation (a–d) and physicochemical characterization of the condensates (e, f). (a) Protein solution (11 g/L, pH 7.8) was adjusted to different ionic strengths at 23 °C by adding NaCl solution with different concentrations, attaining a final protein concentration of 10 g/L. Turbidity of soy glycinin suspensions at different salt concentration are given; the framed cartoons (also in panels b–d) illustrate the emergence of coacervates in the respective phase region. (b) Phase state of soy glycinin as a function of protein concentration at room temperature (23 °C). The pink region delineated by the red circles represents the coacervation region (R2) where phase separation occurs; the blue area outside the blue solid circles is characterized by homogeneous solution. All solutions were prepared via dilution of a stock solution of 100 g/L at pH 7. (c) Influence of pH on the phase boundary of coacervation. Protein solution of 11 g/L with different initial pH was adjusted to different NaCl concentration at 23 °C. (d) Influence of temperature on the phase boundary of coacervation. Protein solution of 11 g/L with initial pH of 8 was adjusted to a different NaCl concentration and kept at a different temperature. The phase diagrams in (b)–(d) were constructed based on the visual appearance of phase separation in the sample as well as detection of microstructures observed under the microscope. (e) Exponential decay of the aspect ratio of coalescing coacervates induced at 0.1 M NaCl of different final diameters, as given in the legend. The fits (solid curves) were used to assess the relaxation time, τ, see SI. The bright field images show the coalescence of two coacervate droplets. The scale bar represents 2 μm. The image sequence is from Movie 1 in the SI. (f) Plot of the relaxation time τ vs the final coacervate diameter. The slope yields the inverse capillary velocity $\eta/\gamma \approx 9.69 \pm 0.53$ s/μm by linear regression ($R^2 = 0.97$, $n = 13$).

globulins, a group of storage proteins sharing a similar structure.[20] Followed by soy glycinin, pea protein and fava bean legumin have recently been reported to form hollow structures through coacervation.[21,22] However, all these studies have not offered a mechanistic view of protein-coacervate-to-hollow-condensate transition. As representative of the 11S globulin family, soy glycinin is a hexamer, and each of its six subunits contains one acidic and one basic polypeptide cross-linked by disulfide bonds[23,24] (see also Figure S1 in the Supporting Information, SI). This structural characteristic represents a substantial difference from coacervation-prone animal proteins featuring mostly one type of polypeptide.[25,26] Here, using soy glycinin as a prototype, we aim at resolving (i) how these molecular characteristics contribute to 11S globulin coacervation and the "unique" transformation into hollow condensates, (ii) what are the driving forces involved in self-assembly during coacervation and cavitation, and (iii) why the coacervates preserve their shape during the phase transition.

https://dx.doi.org/10.1021/acsmacrolett.0c00709
ACS Macro Lett. 2020, 9, 1844–1852

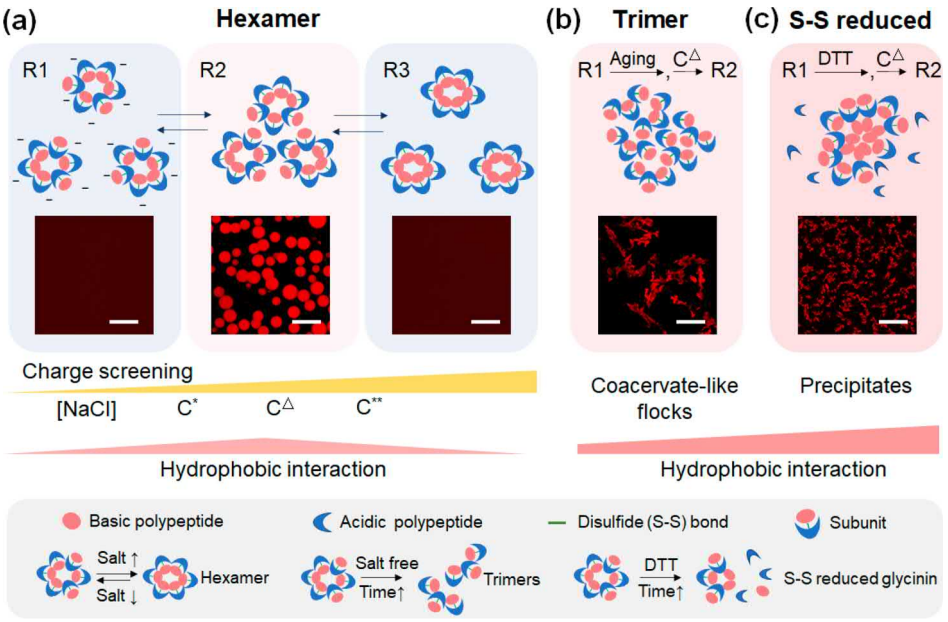

Figure 2. Schematics of the proposed molecular mechanism for soy glycinin coacervation and the structural contribution of the double-trimers stacked hexamer and the disulfide-bonded two-polypeptides subunit. The legend below illustrates the changes at single-molecule level. (a) Effect of changes of the hexamer structure with different exposures of basic and acidic polypeptides induced by altering the ionic strength. Confocal microscopy images of protein suspensions mixed with rhodamine B (which exclusively partitions into the protein-rich phase, see Figure S4) in the three characteristic regions (R1, R2, and R3 in Figure 1) are shown below. Coacervation was induced by mixing freshly prepared protein solution (20 g/L, pH 7.4) with equal volume of 0.2 M NaCl solution to reach C^{Δ} (Figure 1a). (b) Effect of partial dissociation of the protein hexamer into trimer upon aging. Protein solution of 5 g/L was kept at 4 °C for 12 days to induce the dissociation and afterward mixed with equal volume of 0.2 M NaCl solution to reach C^{Δ} (region R2). Instead of fluid coacervate droplets, one observes flocks, see also Figure S7a. (c) Effect of breaking disulfide bonds on coacervation. Protein solution of 10 g/L was incubated with 20 mM DTT for 3h to reduce the disulfide bonds and subsequently mixed with equal volume of 0.2 M NaCl solution to reach C^{Δ} (region R2). The scale bars represent 20 μm.

To shed light on the mechanism of soy glycinin self-coacervation, we first built the phase diagram and explore the coacervate physicochemical characteristics (Figure 1). Homogeneous soy glycinin solutions undergo sequential demixing and mixing phase transitions in response to increasing NaCl concentration (revealed by turbidity measurements), defining three regions in the phase space limited by lower and upper NaCl concentrations, C^* and C^{**}. At [NaCl] < C^* and [NaCl] > C^{**}, the protein solution is homogeneous (regions R1 and R3 in Figure 1a–d). At intermediate concentrations, C^* < [NaCl] < C^{**}, coacervation takes place, leading to phase separation (region R2) with maximum turbidity at around [NaCl] ≈ 0.1 M ≡ C^{Δ} (Figure 1a). The demixing is characterized by random nucleation of spherical dense coacervates, which grow into larger ones via coalescence (see SI, Movie 1). Coalescence is slow and described by an exponential decay with relaxation time τ (Figure 1e), which depends linearly on the size of the coalescing droplets (Figure 1f), see SI, Experimental Section. The proportionality coefficient represents the inverse capillary velocity η/γ,[27] where γ is the interfacial tension driving the coalescence process and η is the droplet viscosity that slows it down. We find $\eta/\gamma \approx 9.69$ s/μm, which corroborates the highly viscous nature of soy glycinin coacervates (see SI, section on coalescence dynamics), also supported by negligible fluorescence recovery after photobleaching (Figure S2).

To understand the observed coacervation process, we consider the hexameric structure of soy glycinin. Every three subunits (each consisting of acidic and basic polypeptides bonded by disulfide bonds) assemble into a trimer, and two trimers stack face to face, forming the hexamer.[23,24] The carboxylic ends of the acidic polypeptides are particularly divergent, also termed the hypervariable region (HVR).[28] One striking feature of the HVR is the high content of negatively charged amino acids with a repeated aspartate/glutamate-rich sequence (Figure S3).[28] The HVR therefore shares the characteristic of the intrinsically disordered regions (IDRs), that is, repetitive amino acid sequences with low complexity, which has been proven to be a crucial structural feature for coacervation to occur.[29,30] Furthermore, the basic polypeptides exhibit a large fraction of hydrophobic amino acids, which are mostly buried inside the protein molecules, while the acidic polypeptides are hydrophilic and mostly exposed.[31,32] The isoelectric point of soy glycinin is around 5.1, implying that it is negatively charged above pH 5.1.[33] Remarkably, with increasing ionic strength, the basic polypeptides become less exposed contrary to the acidic polypeptides.[32]

Considering the above molecular characteristics, in Figure 2, we sketch a plausible structural interpretation of the phase behavior observed in Figure 1. Due to the strong electrostatic repulsion, at pH > 7 and [NaCl] < C^*, the soy glycinin solution remains homogeneous (region R1 in the phase diagram; Figure 2a). Increasing salt concentrations screens the electrostatic repulsion, allowing weak hydrophobic interactions between the exposed hydrophobic basic polypeptides and driving coacervation in region R2 (Figure 2a). This assumption is corroborated by coacervate size decrease observed in the presence of small amounts of urea (Figure S5), which is known to suppress protein–protein hydrophobic interactions.[34,35] However, the coacervation was not disrupted by 1,6-hexanediol, an aliphatic alcohol (Figure S5), which hinders the formation of protein condensates by perturbing weak

https://dx.doi.org/10.1021/acsmacrolett.0c00709
ACS Macro Lett. 2020, 9, 1844–1852

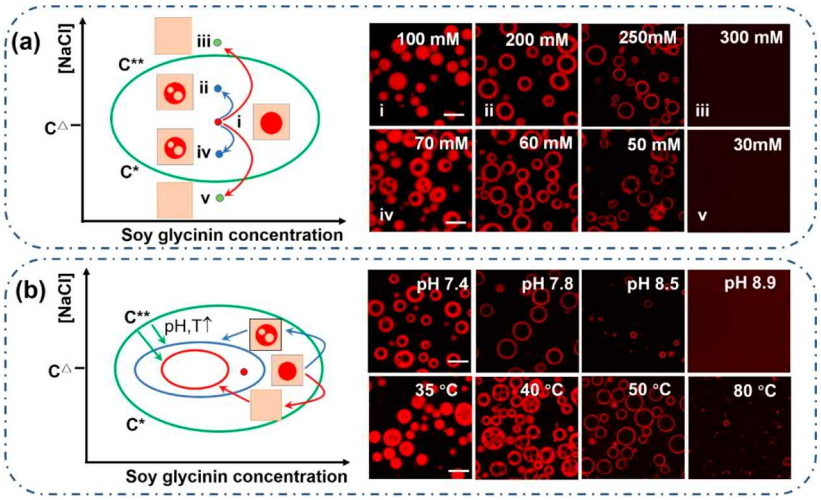

Figure 3. Phase change of soy glycinin coacervates under different solvent conditions and the formation of hollow condensates. The protein coacervates were prepared by mixing protein solution (20 g/L, pH 7.4) with an equal volume of 0.2 M NaCl solution, yielding a final protein concentration of 10 g/L, salt concentration of 0.1 M (C^{Δ}), and pH of 6.85. The environmental condition of the suspension was then adjusted and samples were imaged immediately. (a) Influence of [NaCl] on the coacervate structure. Protein coacervate suspension was adjusted to different NaCl concentrations by mixing with equal volume of NaCl solution (0−500 mM); the final NaCl concentration is indicated in the confocal images. The sketch on the left represents coacervate structure changes in response to shifting of the position in the phase diagram. Examples of the respective locations in the phase diagram (i−v) are illustrated with images on the right. (b) Influence of pH and temperature on the coacervate structure. pH of the coacervate suspension was increased by adding equal volume of NaOH solution (0.5−1.5 mM); the final pH of the suspension is indicated in the images in the upper row. The coacervate suspension (1 mL) was heated via gentle shaking in a water bath under different temperature (indicated in the images, lower row) for 5 min, and the microstructures were observed immediately after heating. The sketch on the left represents how increasing pH or temperature shrinks the phase boundary (green to blue to red ellipses) and the corresponding coacervate structure response, depending on how far it is located to (or out of) the new phase boundary. The scale bars represent 40 μm.

protein−protein interactions.[36] This suggests that hydrophobic interactions of intermediate strength stabilize glycinin coacervates. Tentative interpretation of this stabilization at molecular lever could be sought in the high abundance of glutamine (the most frequent amino acid) and serine in soy glycinin (Figure S6a), both of which were shown to induce hardening and decreased fluidity of protein coacervates.[37] Furthermore, the polyglutamine amino acid sequence (Figure S6b) in the variable region might promote β-sheet structure formation,[38] further contributing to the stabilization of protein droplets.[39] Above C^{**}, the basic polypeptides are mostly shielded in the protein interior, exposing more acidic polypeptides, thus inhibiting coacervation due to the decreased hydrophobic interaction and yielding a homogeneous phase in region R3 (Figure 2a).

We also explored the effect of protein restructuring on the ability to undergo coacervation. Incubation of glycinin solutions at low salt concentration (homogeneous region R1) for a long time (4−12 days) with subsequent addition of salt led to the appearance of coacervate-like flocks (Figure 2b, Figure S7a). This was due to the partial dissociation of the hexameric protein structure into trimers at low ionic strength ([NaCl] < 0.01 M) with time.[40,41] The trimers expose their stacking faces making them more hydrophobic.[23,24] After 12 days, the flocks could not be dissociated when [NaCl] was brought out of the coacervation region R2 (Figure S7b), indicating stronger hydrophobic interaction compared to those in freshly prepared coacervates. We further increased the exposure of hydrophobic basic residues by incubating glycinin with a reducing agent to break the disulfide bonds and release the hydrophilic acidic polypeptides.[42] Then, upon shifting [NaCl] to the coacervation region R2, we observe the transformation of the spherical coacervates to coacervate-like flocks and later on precipitates (Figure 2c and Figure S7c). These precipitates also persist at salt concentrations out of the coacervation region (Figure S7d).

Considering all of the above experiments, we conclude that glycinin coacervation is driven by charge screening of the acidic polypeptides, which promotes weak hydrophobic interactions between the exposed basic polypeptides as typically observed for other proteins.[26,43] The enhanced stability of glycinin droplets against 1,6-hexanediol evidences the presence of even stronger hydrophobic interactions. Importantly, the hexameric structure of glycinin combined with the effect of disulfide bonding shields the basic polypeptides ensuring hydrophobic interaction that is weak enough to induce coacervation rather than flocking or precipitation. Contribution of charge screening to coacervation is further evidenced by the influence of pH on the phase boundary (Figure 1c). Raising the pH above 7 shrinks the phase-separation region R2. At pH > 8.7, coacervation is completely suppressed because of the increased negative surface charge of glycinin,[33] which weakens the screening effect of salt. Below the isoelectric point (~pH 5.1), glycinin becomes positively charged and the electrostatic repulsion increases with decreasing pH.[33] The coacervation is therefore suppressed when pH is below 3.5 (Figure S8). Similarly, increasing temperature from 4 to 50 °C, as shown in Figure 1d, also shrinks the region R2. At T > 55 °C, coacervation is completely suppressed because of the enhanced hydrophobic interaction between soy glycinin molecules that favors the thermally induced irreversible aggregation.[44]

Considering that ionic strength, pH, and temperature significantly influence the coacervation (Figure 1), we hypothesized that soy glycinin coacervates should show responsive structural changes upon modifying these environ-

https://dx.doi.org/10.1021/acsmacrolett.0c00709
ACS Macro Lett. 2020, 9, 1844−1852

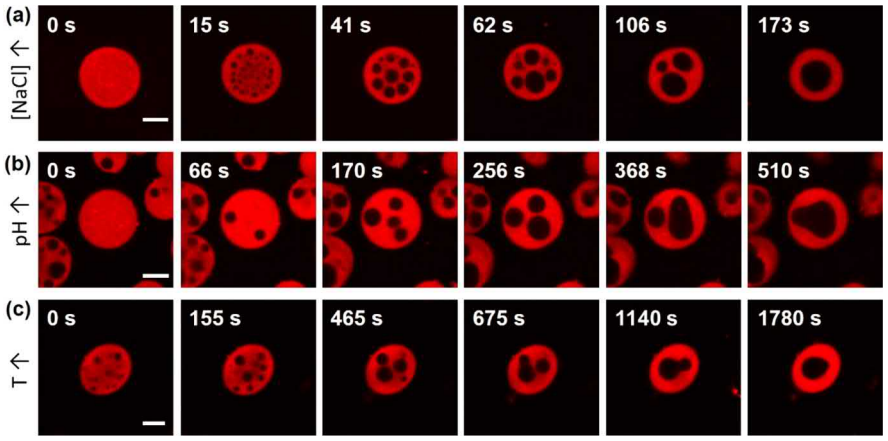

Figure 4. Formation of hollow condensates (cavitation) upon salt, pH or temperature increase. Time-lapse confocal microscopy cross-section images showing cavity formation in the protein condensates under different conditions. Protein coacervates were prepared by mixing protein solution (20 g/L, pH 7.4) with equal volume of 0.2 M NaCl solution at 23 °C, giving a final protein concentration of 10 g/L, NaCl concentration of 0.1 M and pH of 6.85. Ionic strength, pH, and temperature of the suspensions were then adjusted and the corresponding protein-rich phase evolution was visualized by rhodamine B fluorescence shortly after preparation (time 0 corresponds to ∼30 s after salt, pH, or temperature adjustment). (a) The salt concentration of the coacervate suspension was increased from 0.1 to 0.175 M. The image sequence corresponds to Movie 2 in the SI. (b) The pH of the coacervate suspension was increased from to 6.85 to 8.2; Movie 3 in the SI. (c) The coacervate suspension was incubated at 40 °C; Movie 4 in the SI. The scale bars represent 10 μm.

mental conditions. Previous research only reported heat-induced transition from coacervates to hollow condensates. Here, we find that any factor that brings the coacervation system toward the binodals can induce such transition. We consider coacervates formed at [NaCl] = $C^{\Delta} \equiv$ 0.1 M. Upon shifting [NaCl] toward the binodals (C^*/C^{**}), the coacervates transform into hollow condensates with gradually decreasing fraction of the dense phase (Figure 3a) in accordance with the turbidity measurement (Figure 1a). Beyond the phase boundary, the coacervates disperse into a homogeneous phase (Figure 3a). Increasing pH or temperature results in shrinking the coacervation region (R2 in Figure 1c,d), thus, bringing the phase boundary closer to the location of our system in the phase diagram (Figure 3b). The condensates again adjust their phase state by forming a protein-poor phase inside (and transforming the droplets into hollow condensates) or dissolve when the system is beyond the new binodal (Figure 3b). Decreasing protein concentration by dilution could also lead to cavity formation, which is more pronounced when the system is near the coacervation boundary (Figure S9).

We further investigated the process of cavitation as a first step to understand the mechanism of hollow-condensate formation. We prepared protein coacervates at [NaCl] = $C^{\Delta} \equiv$ 0.1 M, and subsequently increased the salt concentration to 0.175 M (i.e., still in region R2 of the phase diagram, Figure 1b). Many small cavities first formed inside the condensates and then merged into a larger one typically within minutes (Figure 4a and Movie 2). Interestingly, cavity formation induced by increasing pH (Figure 4b and Movie 3) or temperature (Figure 4c and Movie 4) follows the same process as that induced by salt. A similar coacervate-to-hollow structure transition has been described for pea protein isolate[21] as well as for RNA−protein (complex) coacervates *in vivo* and *in vitro*,[45−47] although the nature and behavior of the latter as complex coacervates are quite different from those of soy glycinin (simple) coacervates. It should be noted that, for conditions of [NaCl] < C^{Δ}, small irregularly shaped coacervates were often observed (Figure S10). A few seconds of heating would transform them into microdomains with smooth boundaries, followed by the nucleation and growth of protein-poor phase in their interior (Figure S10). This intermediate morphological transition clarifies why irregular coacervate clusters can also form hollow structures upon heating as observed earlier.[48]

The mechanism of hollow-condensate formation is partially related to the interplay of charge screening and hydrophobic interactions. Upon shifting [NaCl] toward C^{**}, the hydrophobic interaction stabilizing the coacervates decreases as more acidic polypeptides are exposed. Both shifting [NaCl] toward C^* and increasing pH enhance the electrostatic repulsion, which weaken the salt screening effects. Increasing temperature leads to a stronger hydrophobic interaction that is unfavorable for coacervation. These changes in the molecular interactions lead to coacervate dissociation, but they do not explain why the protein-poor phase forms in the interior instead of simply shrinking the condensate in size. We speculated that enhanced surface interaction or organization stabilizes the observed shapes. We therefore probed the condensates for structural order (as observed for RNA−protein complexes[45]) using polarization microscopy (Figure 5a). Both coacervates and hollow condensates display strong birefringence at their surface, suggesting surface organization of the protein-rich phase. This liquid-crystalline-like order persists during the transformation into hollow condensates. Interestingly, the inner surface of the hollow condensates also shows birefringence, indicating order. We propose that, at these interfaces, the protein orients so that the more hydrophilic acidic polypeptides extend toward the protein-depleted phase, while the more hydrophobic exposed basic polypeptides extend toward the protein-dense phase, thus, leading to ordered packing (Figure 6). This molecular reorientation presumably strengthens the hydrophobic interactions at these organized surfaces, which is supported by the observation that, in the presence of urea, coacervate or hollow-condensate dissolution initiates from the dense phase to the surface (Figure S11). The surface order and increased protein

https://dx.doi.org/10.1021/acsmacrolett.0c00709
ACS Macro Lett. 2020, 9, 1844−1852

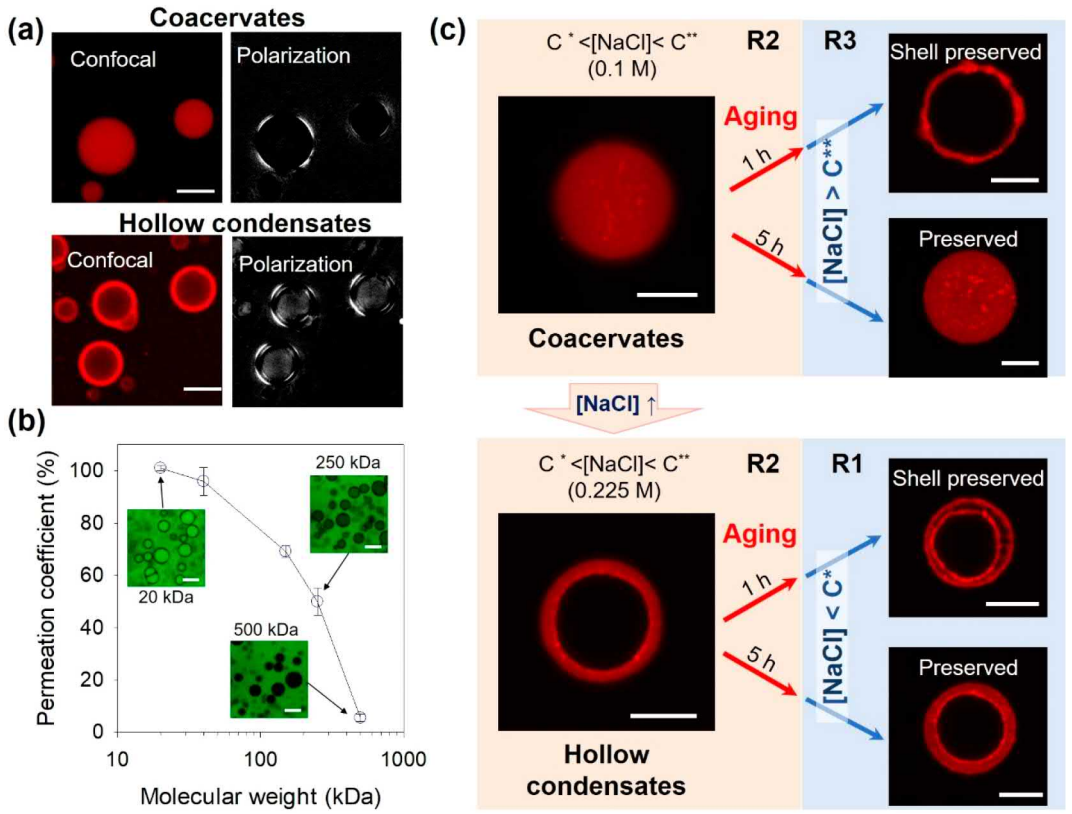

Figure 5. Structural order at coacervate and hollow-condensate surfaces, mesh size of surface and dense phase and aging conditions for preserved topology beyond the coacervation region R2. Protein coacervates were prepared by mixing soy glycinin solution (20 g/L, pH 7.4) with equal volume of 0.2 M NaCl solution at 23 °C to yield a protein suspension with protein concentration of 10 g/L and NaCl concentration of 0.1 M. Hollow condensates were induced by increasing the ionic strength to 0.225 M. (a) Optical images of coacervates and hollow condensates with cross-polarizing light show birefringence, indicating molecular ordering at the outer and cavity surfaces. Corresponding fluorescence micrographs are also shown. The scale bars represent 20 μm. (b) Permeation coefficient of FITC-labeled dextran as a function of molecular weight (see Figure S14 for details on the measurement). The measurements were performed on hollow condensates (n = 5). The error bars indicate standard deviation. The inserts show representative images of the permeation of dextran in the hollow coacervates. The scale bars represent 40 μm. (c) Influence of aging on the stability of coacervates and hollow condensates upon shifts beyond the phase boundary of the coacervation region R2; see more details in Figure S15. Aging was done at 23 °C under mild stirring and for different periods (indicated above the red arrows), after which the salt concentration of the suspension was shifted to 0.03 M, which falls into the homogeneity region R1, that is, [NaCl] < C^*, or 0.3 M, which falls into homogeneity region R3, that is, [NaCl] > C^{**}. The scale bars represent 10 μm.

interactions could contribute to the long stability of the hollow condensates (Figure S12), as discussed below.

Considering that part of the glycinin molecules in the coacervate interior become mobile and are released out of the coacervates upon cavitation, the dense phase and ordered surface should have a mesh size that allows the diffusion of free glycinin. We probed this mesh size using FITC-labeled dextran. Dextran, with a M_w > 4 kDa, was practically excluded from the protein-rich phase of the coacervates or the hollow condensates (Figures S13 and S14). Upon cavity formation, low-molecular-weight dextran (≤40 kDa) could diffuse through the capsule-like dense phase, while 500 kDa dextran could not permeate (Figures 5b and S14). Presumably, the ordered surface acts as a size-dependent filter with a mesh size of at least 3−5 nm, as defined by the radius of gyration of 20−40 kDa dextran,[49] that would therefore allow free glycinin, which has a radius around 4 nm[50,51] to leak out rather than concentrating in the layer of protein-dense phase.

Soy proteins tend to aggregate and gel even at low temperature, promoted by increasing protein concentration.[52,53] Considering that the condensates represent a highly dense protein phase, it is plausible that protein−protein interactions are enhanced with time. To resolve the influence of aging and probe the stability of the resulting structures, we aged protein coacervates at 23 °C for different periods and subsequently examined their stability by shifting the salt concentration out of the coacervation region R2 and into the homogeneity regions (R1/R3). We were, thus, able to resolve aging conditions that lead to preserving the structures. After a short aging time, the coacervates could still be dissociated irrespective of the [NaCl] shift direction (Figure S15a). In samples aged for 1 h, the coacervate surface retained its topology (Figure 5c, upper panel) in region R3, suggesting stronger protein−protein interactions resulting from the surface order evidenced by the polarization microscopy images (Figure 5a). At longer times (>5 h), the whole coacervate appeared preserved (Figure 5c, upper panel).

Aging also strengthened the stability of hollow condensates. Short aging times (∼10 min) led to thinning of the protein-dense phase or partial dissolution (Figure S15b). After aging for 1 h, the dense phase was released, leaving the outer and inner surfaces of the hollow condensates as concentric shells in region R1 (Figure 5c, lower panel, and Figure S15b). This confirms that protein molecules at the inner surface of the

https://dx.doi.org/10.1021/acsmacrolett.0c00709
ACS Macro Lett. 2020, 9, 1844−1852

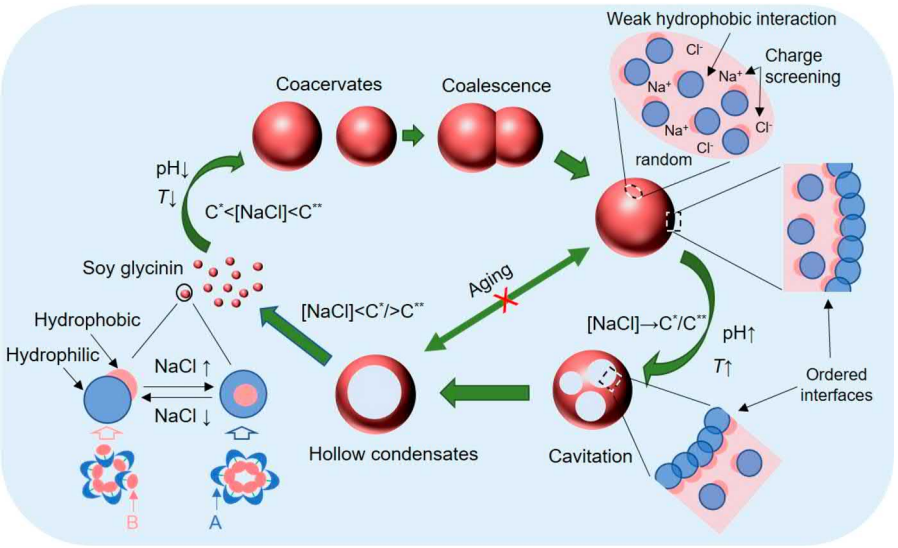

Figure 6. Schematic illustration of the mechanisms of the self-coacervation of soy glycinin, the transformation from coacervates to hollow condensates and their surface organization. The hexameric structure of glycinin contributes to these phase changes via the interplay of the basic (B, hydrophobic) and acidic (A, hydrophilic) polypeptides, which modulate the protein−protein interactions upon environmental condition changes, as shown in Figure 2. The structure of the hexamer was simplified with one hydrophilic part (blue), representing the exposed acidic polypeptides and one hydrophobic part (pink), representing the exposed basic polypeptides. Homogeneous solutions of the protein (left) undergo coacervation in a specific range of salt concentration ($C^* < [NaCl] < C^{**}$), pH, and temperature, which is driven by charge screening of acidic polypeptides and the hydrophobic interaction between exposed basic polypeptides. The coacervates are fluid and can grow via coalescence. Upon changes in the external conditions bringing the system closer to the binodal (C^* or C^{**}) or upon increasing temperature or pH, the coacervates develop cavities of the protein-poor phase, which transforms the droplets into hollow condensates. This process is irreversible and is hindered by aging. The amphiphilic glycinin molecules orient at condensate interface, rendering surface order that strengthens intermolecular interactions stabilizing the coacervate shape. In fresh solutions, the dense phase dissolves once the external conditions shift the system out of the region of phase coexistence, while in aged ones, the structures are preserved.

hollow condensates assemble similar to those at the outer surface, in accordance with the polarization microscopy observations. Overall, aging led to the formation of stabilized shells offering a facile alternative pathway for microcapsule production. The enhanced stability with aging is presumably due to the large abundance of glutamine and serine (Figure S6a), which promotes the hardening of coacervates in a time-dependent manner.[37] The polyglutamine sequence might also contribute to the stabilization of protein droplets by forming higher-order structure (Figure S6b).[38] Overall, the hydrophobic interactions are strengthened with aging (Figure S16).

The proposed molecular mechanism behind coacervate formation, transformation into hollow-condensates, and shape stability is summarized in Figure 6. Remarkably, aging enhances the protein−protein interaction, transforming the coacervates or hollow condensates into microcapsules with a morphology stable to solvent condition changes. This research provides essential knowledge and approaches for investigating the coacervation of other plant seed 11S globulins. Furthermore, it paves the way toward designing novel microstructures such as semipermeable responsive microcapsules as well as further understanding of the accumulation and dissociation of the protein condensates in plant seed cells.[54,55]

■ ASSOCIATED CONTENT

Supporting Information

The Supporting Information is available free of charge at https://pubs.acs.org/doi/10.1021/acsmacrolett.0c00709.

Details for the materials and experimental methods, supporting figures, and movie captions (PDF)

Movie 1: Coalescence dynamics of protein coacervates (MP4)

Movie 2: Transition from coacervates to hollow condensates induced by increasing ionic strength (AVI)

Movie 3: Transition from coacervates to hollow condensates induced by increasing pH (AVI)

Movie 4: Transition from coacervates to hollow condensates induced by increasing temperature (AVI)

■ AUTHOR INFORMATION

Corresponding Authors

Nannan Chen − *Guangdong Saskatchewan Oilseed Joint Laboratory, Department of Food Science and Engineering, Jinan University, 510632 Guangzhou, China; Max Planck Institute of Colloids and Interfaces, Department of Theory and Bio-Systems, 14424 Potsdam, Germany*; Email: nannanchen@jnu.edu.cn

Rumiana Dimova − *Max Planck Institute of Colloids and Interfaces, Department of Theory and Bio-Systems, 14424 Potsdam, Germany*; orcid.org/0000-0002-3872-8502; Email: rumiana.dimova@mpikg.mpg.de

Authors

Ziliang Zhao − *Max Planck Institute of Colloids and Interfaces, Department of Theory and Bio-Systems, 14424 Potsdam, Germany*; orcid.org/0000-0002-8723-7312

Yong Wang − *Guangdong Saskatchewan Oilseed Joint Laboratory, Department of Food Science and Engineering, Jinan University, 510632 Guangzhou, China*; orcid.org/0000-0001-7547-1542

https://dx.doi.org/10.1021/acsmacrolett.0c00709
ACS Macro Lett. 2020, 9, 1844−1852

Complete contact information is available at:
https://pubs.acs.org/10.1021/acsmacrolett.0c00709

Notes

The authors declare no competing financial interest.

■ ACKNOWLEDGMENTS

N.C. acknowledges support from China Postdoctoral Innovation Talent Support Program (BX20190145), China Postdoctoral Science Foundation (2019M663387), and Natural Science Foundation of Guangdong Province (2019A1515011176). Z.Z. and R.D. thank the MaxSynBio consortium, which is jointly funded by the Federal Ministry of Education and Research (BMBF) of Germany and the Max Planck Society (MPG). We thank N. Yandrapalli for assistance with polarization microscopy and Jun Zhu for the SDS-PAGE.

■ REFERENCES

(1) Alberti, S.; Gladfelter, A.; Mittag, T. Considerations and Challenges in Studying Liquid-Liquid Phase Separation and Biomolecular Condensates. *Cell* **2019**, *176* (3), 419−434.
(2) Mohanty, B.; Bohidar, H. B. Systematic of Alcohol-Induced Simple coacervation in Aqueous Gelatin Solutions. *Biomacromolecules* **2003**, *4*, 1080−1086.
(3) Croguennec, T.; Tavares, G. M.; Bouhallab, S. Heteroprotein complex coacervation: A generic process. *Adv. Colloid Interface Sci.* **2017**, *239*, 115−126.
(4) Mitrea, D. M.; Kriwacki, R. W. Phase separation in biology; functional organization of a higher order. *Cell Commun. Signaling* **2016**, *14*, 1.
(5) Banani, S. F.; Lee, H. O.; Hyman, A. A.; Rosen, M. K. Biomolecular condensates: organizers of cellular biochemistry. *Nat. Rev. Mol. Cell Biol.* **2017**, *18* (5), 285−298.
(6) Mohammadi, P.; Aranko, A. S.; Lemetti, L.; Cenev, Z.; Zhou, Q.; Virtanen, S.; Landowski, C. P.; Penttilä, M.; Fischer, W. J.; Wagermaier, W.; Linder, M. B. Phase transitions as intermediate steps in the formation of molecularly engineered protein fibers. *Commun. Biol.* **2018**, *1* (1), 86.
(7) Kim, S.; Yoo, H. Y.; Huang, J.; Lee, Y.; Park, S.; Park, Y.; Jin, S.; Jung, Y. M.; Zeng, H.; Hwang, D. S.; Jho, Y. Salt Triggers the Simple Coacervation of an Underwater Adhesive When Cations Meet Aromatic pi Electrons in Seawater. *ACS Nano* **2017**, *11* (7), 6764−6772.
(8) Black, K. A.; Priftis, D.; Perry, S. L.; Yip, J.; Byun, W. Y.; Tirrell, M. Protein Encapsulation via Polypeptide Complex Coacervation. *ACS Macro Lett.* **2014**, *3* (10), 1088−1091.
(9) Nishinari, K.; Fang, Y.; Guo, S.; Phillips, G. O. Soy proteins: A review on composition, aggregation and emulsification. *Food Hydrocolloids* **2014**, *39*, 301−318.
(10) Renkema, J. M. S.; Gruppen, H.; Van Vliet, T. Influence of pH and ionic strength on heat-induced formation and rheological properties of soy protein gels in relation to denaturation and their protein compositions. *J. Agric. Food Chem.* **2002**, *50*, 6064−6071.
(11) Mo, X.; Zhong, Z.; Wang, D.; Sun, X. Soybean Glycinin Subunits: Characterization of Physicochemical and Adhesion Properties. *J. Agric. Food Chem.* **2006**, *54*, 7589−7593.
(12) Chen, N.; Zhao, M.; Nicolai, T.; Chassenieux, C. Exploiting Salt Induced Microphase Separation To Form Soy Protein Microcapsules or Microgels in Aqueous Solution. *Biomacromolecules* **2017**, *18* (7), 2064−2072.
(13) Chen, N.; Zhang, J.; Mei, L.; Wang, Q. Ionic Strength and pH Responsive Permeability of Soy Glycinin Microcapsules. *Langmuir* **2018**, *34* (33), 9711−9718.
(14) Nesterenko, A.; Alric, I.; Silvestre, F.; Durrieu, V. Vegetable proteins in microencapsulation: A review of recent interventions and their effectiveness. *Ind. Crops Prod.* **2013**, *42*, 469−479.
(15) Can Karaca, A.; Low, N. H.; Nickerson, M. T. Potential use of plant proteins in the microencapsulation of lipophilic materials in foods. *Trends Food Sci. Technol.* **2015**, *42* (1), 5−12.
(16) Lazko, J.; Popineau, Y.; Legrand, J. Soy glycinin microcapsules by simple coacervation method. *Colloids Surf., B* **2004**, *37* (1−2), 1−8.
(17) Li, X.; Erni, P.; van der Gucht, J.; de Vries, R. Encapsulation Using Plant Proteins: Thermodynamics and Kinetics of Wetting for Simple Zein Coacervates. *ACS Appl. Mater. Interfaces* **2020**, *12* (13), 15802−15809.
(18) Zhao, H.; Guo, M.; Ma, X.; Ding, T.; Liu, D. Microstructure and permeability of hollow microcapsules produced from faba bean 11s protein. *Food Hydrocolloids* **2021**, *112*, 106292.
(19) Tong, W.; Song, X.; Gao, C. Layer-by-layer assembly of microcapsules and their biomedical applications. *Chem. Soc. Rev.* **2012**, *41*, 6103−6124.
(20) Tandang-Silvas, M. R.; Fukuda, T.; Fukuda, C.; Prak, K.; Cabanos, C.; Kimura, A.; Itoh, T.; Mikami, B.; Utsumi, S.; Maruyama, N. Conservation and divergence on plant seed 11S globulins based on crystal structures. *Biochim. Biophys. Acta, Proteins Proteomics* **2010**, *1804* (7), 1432−1442.
(21) Cochereau, R.; Nicolai, T.; Chassenieux, C.; Silva, J. V. C. Mechanism of the spontaneous formation of plant protein microcapsules in aqueous solution. *Colloids Surf., A* **2019**, *562*, 213−219.
(22) Zhao, H.; Zhou, X.; Wang, J.; Ma, X.; Guo, M.; Liu, D. Heat-induced hollow microcapsule formation using fava bean legumin. *Food Hydrocolloids* **2021**, *112*, 106207.
(23) Adachi, M.; Kanamori, J.; Masuda, T.; Yagasaki, K.; Kitamura, K.; Mikami, B.; Utsumi, S. Crystal structure of soybean 11S globulin: Glycinin A3B4 homohexamer. *Proc. Natl. Acad. Sci. U. S. A.* **2003**, *100*, 7395−7400.
(24) Adachi, M.; Takenaka, Y.; Gidamis, A. B.; Mikami, B.; Utsumi, S. Crystal structure of soybean proglycinin A1aB1b homotrimer. *J. Mol. Biol.* **2001**, *305* (2), 291−305.
(25) Gabryelczyk, B.; Cai, H.; Shi, X.; Sun, Y.; Swinkels, P. J. M.; Salentinig, S.; Pervushin, K.; Miserez, A. Hydrogen bond guidance and aromatic stacking drive liquid-liquid phase separation of intrinsically disordered histidine-rich peptides. *Nat. Commun.* **2019**, *10* (1), 5465.
(26) Wei, W.; Tan, Y.; Martinez Rodriguez, N. R.; Yu, J.; Israelachvili, J. N.; Waite, J. H. A mussel-derived one component adhesive coacervate. *Acta Biomater.* **2014**, *10* (4), 1663−1670.
(27) Eggers, J.; Lister, J. R.; Stone, H. A. Coalescence of liquid drops. *J. Fluid Mech.* **1999**, *401*, 293−310.
(28) Nielsen, N. C.; Dickinson, C. D.; Cho, T.-J.; Thanh, V. H.; Scallon, B. J.; Fischer, R. L.; Sims, T. L.; Drews, C. N.; Goldberg, R. B. Characterization of the glycinin gene family in soybean. *Plant Cell* **1989**, *1*, 313−328.
(29) Majumdar, A.; Dogra, P.; Maity, S.; Mukhopadhyay, S. Liquid-Liquid Phase Separation Is Driven by Large-Scale Conformational Unwinding and Fluctuations of Intrinsically Disordered Protein Molecules. *J. Phys. Chem. Lett.* **2019**, *10* (14), 3929−3936.
(30) Schuster, B. S.; Dignon, G. L.; Tang, W. S.; Kelley, F. M.; Ranganath, A. K.; Jahnke, C. N.; Simpkins, A. G.; Regy, R. M.; Hammer, D. A.; Good, M. C.; Mittal, J. Identifying sequence perturbations to an intrinsically disordered protein that determine its phase-separation behavior. *Proc. Natl. Acad. Sci. U. S. A.* **2020**, *117* (21), 11421−11431.
(31) Yuan, D.-B.; Yang, X.-Q.; Tang, C.-H.; Zheng, Z.-X.; Wei, M.; Ahmad, I.; Yin, S.-W. Physicochemical and functional properties of acidic and basic polypeptides of soy glycinin. *Food Res. Int.* **2009**, *42* (5−6), 700−706.
(32) Lakemond, C. M. M.; de Jongh, H. H. J.; Hessing, M.; Gruppen, H.; Voragen, A. G. J. Soy glycinin: Influence of pH and ionic strength on solubility and molecular structure at ambient temperatures. *J. Agric. Food Chem.* **2000**, *48*, 1985−1990.
(33) Yuan, Y.; Wan, Z.-L.; Yang, X.-Q.; Yin, S.-W. Associative interactions between chitosan and soy protein fractions: Effects of pH,

mixing ratio, heat treatment and ionic strength. *Food Res. Int.* **2014**, *55*, 207−214.
(34) Kim, J. R.; Muresan, A.; Lee, K. Y.; Murphy, R. M. Urea modulation of beta-amyloid fibril growth: experimental studies and kinetic models. *Protein Sci.* **2004**, *13* (11), 2888−2898.
(35) Li, H. R.; Chen, T. C.; Hsiao, C. L.; Shi, L.; Chou, C. Y.; Huang, J. R. The physical forces mediating self-association and phase-separation in the C-terminal domain of TDP-43. *Biochim. Biophys. Acta, Proteins Proteomics* **2018**, *1866* (2), 214−223.
(36) Ambadipudi, S.; Reddy, J. G.; Biernat, J.; Mandelkow, E.; Zweckstetter, M. Residue-specific identification of phase separation hot spots of Alzheimer's-related protein tau. *Chem. Sci.* **2019**, *10* (26), 6503−6507.
(37) Wang, J.; Choi, J. M.; Holehouse, A. S.; Lee, H. O.; Zhang, X.; Jahnel, M.; Maharana, S.; Lemaitre, R.; Pozniakovsky, A.; Drechsel, D.; Poser, I.; Pappu, R. V.; Alberti, S.; Hyman, A. A. A Molecular Grammar Governing the Driving Forces for Phase Separation of Prion-like RNA Binding Proteins. *Cell* **2018**, *174* (3), 688−699.
(38) Darnell, G.; Orgel, J. P.; Pahl, R.; Meredith, S. C. Flanking polyproline sequences inhibit beta-sheet structure in polyglutamine segments by inducing PPII-like helix structure. *J. Mol. Biol.* **2007**, *374* (3), 688−704.
(39) Lin, Y.; Protter, D. S.; Rosen, M. K.; Parker, R. Formation and Maturation of Phase-Separated Liquid Droplets by RNA-Binding Proteins. *Mol. Cell* **2015**, *60* (2), 208−219.
(40) Wolf, W. J.; Briggs, D. R. Studies on the cold insoluble fraction of the water extractable soybean proteins. II. Factors influencing conformation changes in the 11 S Component. *Arch. Biochem. Biophys.* **1958**, *76*, 377−393.
(41) Wolf, W. J.; Rackis, J. J.; Smith, A. K.; Sasame, H. A.; Babcock, G. E. Behavior of the 11S Protein of soybeans in acid solutions. I. Effects of pH, ionic strength and time on ultracentrifugal and optical rotatory properties. *J. Am. Chem. Soc.* **1958**, *80*, 5730−5735.
(42) Wolf, W. J. Sulfhydryl content of glycinin: effect of reducing agents. *J. Agric. Food Chem.* **1993**, *41*, 168−176.
(43) Cai, H.; Gabryelczyk, B.; Manimekalai, M. S. S.; Grüber, G.; Salentinig, S.; Miserez, A. Self-coacervation of modular squid beak proteins − a comparative study. *Soft Matter* **2017**, *13* (42), 7740−7752.
(44) Guo, J.; Yang, X. Q.; He, X. T.; Wu, N. N.; Wang, J. M.; Gu, W.; Zhang, Y. Y. Limited aggregation behavior of beta-conglycinin and its terminating effect on glycinin aggregation during heating at pH 7.0. *J. Agric. Food Chem.* **2012**, *60* (14), 3782−3791.
(45) Alshareedah, I.; Moosa, M. M.; Raju, M.; Potoyan, D. A.; Banerjee, P. R. Phase transition of RNA−protein complexes into ordered hollow condensates. *Proc. Natl. Acad. Sci. U. S. A.* **2020**, *117*, 15650−15658.
(46) Kistler, K. E.; Trcek, T.; Hurd, T. R.; Chen, R.; Liang, F.-X.; Sall, J.; Kato, M.; Lehmann, R. Phase transitioned nuclear Oskar promotes cell division of Drosophila primordial germ cells. *eLife* **2018**, *7*, e37949.
(47) Banerjee, P. R.; Milin, A. N.; Moosa, M. M.; Onuchic, P. L.; Deniz, A. A. Reentrant Phase Transition Drives Dynamic Substructure Formation in Ribonucleoprotein Droplets. *Angew. Chem., Int. Ed.* **2017**, *56* (38), 11354−11359.
(48) Zhao, H. H.; Guo, M. M.; Ding, T.; Ye, X. Q.; Liu, D. H. Exploring the mechanism of hollow microcapsule formation by self-assembly of soy 11s protein upon heating. *Food Hydrocolloids* **2020**, *108*, 105379.
(49) Andrieux, K.; Lesieur, P.; Lesieur, S.; Ollivon, M.; Grabielle-Madelmont, C. c. Characterization of Fluorescein Isothiocyanate-Dextrans Used in Vesicle Permeability Studies. *Anal. Chem.* **2002**, *74*, 5217−5226.
(50) Badley, A. R.; Atkinson, D.; Hauser, H.; Oldani, D.; Green, J. P.; Stubbs, J. M. The structure, physical and chemical properteis of soy bean protein glycinin. *Biochim. Biophys. Acta, Protein Struct.* **1975**, *412*, 214−228.
(51) Sokolova, A.; Kealley, C. S.; Hanley, T.; Rekas, A.; Gilbert, E. P. Small-angle X-ray scattering study of the effect of pH and salts on 11S soy glycinin in the freeze-dried powder and solution states. *J. Agric. Food Chem.* **2010**, *58* (2), 967−974.
(52) Chen, N.; Zhao, M.; Chassenieux, C.; Nicolai, T. The effect of adding NaCl on thermal aggregation and gelation of soy protein isolate. *Food Hydrocolloids* **2017**, *70*, 88−95.
(53) Chen, N.; Nicolai, T.; Chassenieux, C.; Wang, Y. pH and ionic strength responsive core-shell protein microgels fabricated via simple coacervation of soy globulins. *Food Hydrocolloids* **2020**, *105*, 105853.
(54) Dawidowicz-Grzegorzewska, A. Degradation of Protein and Lipid Bodies during Dormancy Removal in Apple Seeds. *J. Plant Physiol.* **1989**, *135* (1), 43−51.
(55) Mori, T.; Maruyama, N.; Nishizawa, K.; Higasa, T.; Yagasaki, K.; Ishimoto, M.; Utsumi, S. The composition of newly synthesized proteins in the endoplasmic reticulum determines the transport pathways of soybean seed storage proteins. *Plant J.* **2004**, *40* (2), 238−249.

https://dx.doi.org/10.1021/acsmacrolett.0c00709
ACS Macro Lett. 2020, 9, 1844−1852

Supporting information

Resolving the mechanisms of soy glycinin self-coacervation and hollow-condensate formation

Nannan Chen,*[,1,2] Ziliang Zhao,[2] Yong Wang,[1] Rumiana Dimova*[,2]

[1]*Guangdong Saskatchewan Oilseed Joint Laboratory, Department of Food Science and Engineering, Jinan University, 510632 Guangzhou, China*

[2]*Max Planck Institute of Colloids and Interfaces, Department of Theory & Bio-Systems, Science Park Golm, 14424 Potsdam, Germany*

Corresponding authors:

*nannanchen@jnu.edu.cn

*Rumiana.Dimova@mpikg.mpg.de

Materials

Defatted 7B soy flour was kindly provided by Archer Daniels Midland Company, United States. Rhodamine B, fluorescein isothiocyanate isomer (FITC), FITC-dextran (4, 10, 20, 40, 150, 250 and 500 kDa), protein marker, bovine serum albumin (BSA), sodium hydroxide (NaOH), sodium bisulfite, dithiothreitol (DTT), dimethyl sulfoxide (DMSO) and urea were obtained from Sigma-Aldrich (St. Louis, Missouri, United States). Sodium chloride (NaCl) and hydrochloric acid (HCl) were obtained from Carl Roth GmbH + Co.KG (Karlsruhe, Germany). Millipore water was used for all solution preparations.

Experimental section

Isolation of soy glycinin. Preparation of glycinin followed the method of Nagano et al. with slight modifications.[1] Briefly, the defatted soy flour was dispersed in 15-fold water in weight and adjusted to pH 7.5 with 2 M NaOH. This slurry was then centrifuged (9000×*g*, 30 min) at 4 °C. Dry sodium bisulfite (SBS) was then added to the supernatant (0.98 g SBS/L), the pH of the solution was adjusted to 6.4 with 2 M HC1, and the obtained turbid dispersion was kept at 4 °C overnight. After that, the dispersion was centrifuged (6500×*g*, 30 min) at 4 °C. The precipitates which consisted predominantly of glycinin were dispersed in 5-fold water and the pH was adjusted to 7. The glycinin solution was then dialyzed against Millipore water for two days at 4 °C and then

freeze-dried to acquire the final product. SDS-PAGE analysis (**Figure S1**) shows that the purity of the glycinin is 97.5%.

Coating of coverslips for microscopy observation. In order to prevent the wetting and spreading of the coacervates on the coverslip, the coverslip was coated with bovine serum albumin (BSA). BSA solution of 10 g/L in water was prepared. The coverslip was washed with ethanol and water, sequentially. Then it was dried under nitrogen flow. A droplet (50 μL) of BSA solution was deposited and spread evenly onto the coverslip (26×56 mm, Waldemar Knittel Glasbearbeitungs GmbH, Germany) with a pipette tip and kept at room temperature until drying. The dried surface of the coated side was washed with small amount of Millipore water and then dried using nitrogen flow.

Microscopy observation chamber. The chamber for microscopy observation consisted of two coverslips pressed against an adhesive rubber spacer with a thickness of 3 mm. The lateral dimension of the bottom coverslip was 26×56 mm with a thickness of 0.17±0.01 mm which was coated by BSA, and the top coverslip had lateral dimension of 22×22 mm and its thickness was 0.17±0.01 mm. Before measurement, a droplet of 20 μL sample was transferred onto the coverslip and then sealed by the top coverslip with the spacer in the middle.

Phase diagrams. Soy glycinin solutions with different concentrations were prepared from a stock solution at C = 100 g/L and pH 7. The protein solution was set to different pH by adding 0.1 M HCl or NaOH and to different temperature by incubating the suspension in a water bath. The NaCl concentration of the protein solutions was then set by adding aliquots of a concentrated NaCl solution (0.2 to 4 M) with the same temperature as the protein solution. All the protein suspensions were incubated at different temperature for 18 h to ensure complete phase separation. The binodal NaCl concentrations (C^* and C^{**}) were determined either by direct visual observation for presence of two phases in the sample vial for suspensions with protein concentration $\geqslant$ 5 g/L or by observation under a microscope in bright field mode using a water immersion objective (63×/1.2NA) on Zeiss Axio Observer microscope for suspensions with protein concentration < 5 g/L. We confirmed that results from visual observation of the sample are consistent with the microscopy data.

Turbidity measurement. The turbidity of the soy glycinin solutions was determined by measuring the absorbance of the suspension at 500 nm immediately after sample preparation using Unicam UV-Vis Spectrometer (Thermo Scientific, United States). Cuvettes with path lengths of 0.5 cm were used. Contrary to the measurements used for building the phase diagram, no incubation for longer times was done because of sedimentation of the droplets.

Confocal laser scanning microscopy (CLSM) and polarization microscopy. Rhodamine B or FITC-dextran were mixed with glycinin suspension to a final concentration of 5 mg/L or 1 g/L, to visualize the protein dense phase or probe the mesh size of the condensates, respectively. The suspension was immediately placed in an observation chamber. The suspension was examined for the presence of microstructures at 23 °C with a confocal laser scanning microscope (SP5 DMI 6000, Leica Microsystems Heidelberg GmbH, Germany) using a water immersion objective (63×/1.2NA). The polarization images were taken by a confocal laser scanning microscope (SP8, Leica Microsystems Heidelberg GmbH, Germany) equipped with polarizers; 20×/0.4NA objective was used.

Coalescence dynamics. Coalescence dynamics of protein coacervates was investigated following an approach of Brangwynne et al. with slight modifications.[2] The aspect ratio of protein

coacervates was determined by fitting an ellipse to the shape and calculating a/b, where a and b are the long and short axes of the ellipse. For analysis of fusing coacervates, the time evolution of this aspect ratio was fitted to a function of the form $a/b = 1 + (a_0/b_0 - 1) \cdot exp(-t/\tau)$, where t is time, τ is the characteristic relaxation time, and a_0/b_0 is the initial aspect ratio. We define the length scale of these fusing coacervates using the final diameter of the coacervates a_f. Plots of τ vs. a_f were fitted to a line of the form $\tau = \frac{\eta}{\gamma} a_f$, to determine the inverse capillary velocity η/γ. Note that we considered only droplets of similar sizes to reduce the scatter in the data and to reflect the assumptions of the model for droplets with identical radii.[3] The measurements were done with Zeiss Axio Observer Microscope using the bright field mode equipped with Hamamatsu ORCA R2 CCD camera. A water immersion objective (63×/1.2NA) was used.

The obtained data (**Figure 1e,f**) yield for the inverse capillary velocity $\eta/\gamma \approx 9.69$ s/μm. Theoretical arguments and experiment work (see e.g. references in [4]) suggest that the interfacial tension is $\gamma \approx k_B T/d^2$, where $k_B T$ is the thermal energy and d is a typical length scale. If we assume $d \approx 5$ nm for the glycinin molecule,[5, 6] we estimate $\gamma \approx 0.16$ mN/m, yielding for the droplet viscosity $\eta \approx 1.6$ kPa.s. This extremely high viscosity is consistent with the very slow molecular diffusion as revealed from fluorescence recovery after photobleaching (FRAP) measurements, showing almost no recovery within minutes (**Figure S2**).

Protein labeling. Labeling of soy glycinin with fluorescein isothiocyanate isomer (FITC) was performed according to the method reported by Sağlam et al. with modification.[7] A 20 g/L soy glycinin solution was prepared in 0.1 M carbonate buffer (pH 9). FITC was dissolved in DMSO at 4 g/L. FITC solution was slowly added into the protein solution with gentle stirring to a final concentration of 0.2 g/L. The sample was incubated in the dark while stirring at 23 ºC for 3 h. The protein solution was then dialyzed against Millipore water in the dark at 4 ºC for 60 h to remove excess FITC. Millipore water was refreshed every 12 h. The pH of the labeled protein solution was adjusted to 7.4 by adding 0.1 M NaOH and this labeled protein solution was used for FRAP measurement.

Fluorescence recovery after photo bleaching (FRAP). FRAP measurements were performed on Leica SP8 confocal laser scanning microscope equipped with a FRAP booster. Coacervation of the soy glycinin was triggered by mixing protein solution (5 g/L) with equal volume of 0.2 M NaCl giving a final protein concentration of 2.5 g/L and salt concentration of 0.1 M. FITC-soy glycinin accounted for 10% of the total protein concentration. Circular region of interest (ROI) with diameter of 2 μm on the coacervate droplet (8 μm in diameter) was bleached using 3 iterative pulses of total time ~3 s using the Argon laser at 488 nm. Fluorescence intensities from ROI corresponding to photobleaching were analyzed using ImageJ.

Electrophoresis. Reducing sodium dodecyl sulfate-polyacrylamide gel electrophoresis (SDS-PAGE) was performed on a discontinuous buffered system, using 12% separating gel. The protein sample was mixed with 5× reducing sample buffer which contained β-mercaptoethanol and then heated at 90 °C for 10 min. After the electrophoresis, the gel was stained using InstantBlue™ solution for 1 h and then rinsed with Millipore water. The protein composition was analyzed by measuring the brightness of the bands using ImageJ.

Supporting Figures

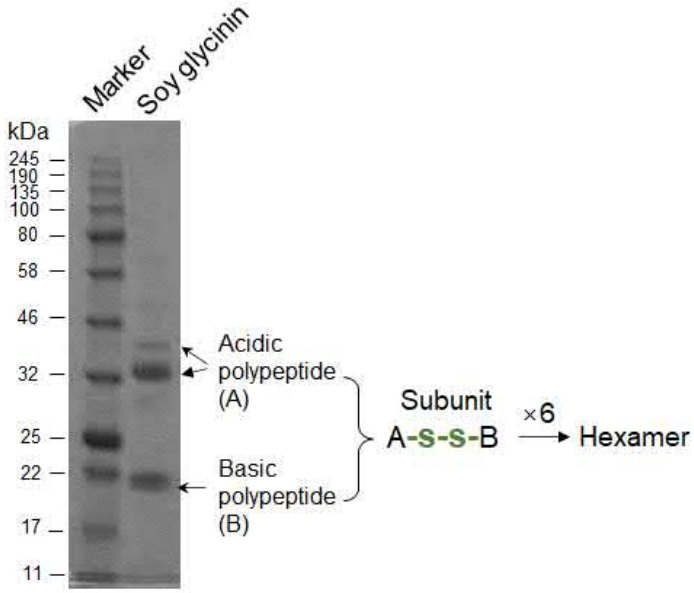

Figure S1. Reducing SDS-PAGE of soy glycinin. ImageJ analysis shows the purity of the soy glycinin to be 97.5%. The small amount of contamination is β-conglycinin, the other major component of soy protein. Soy glycinin is hexamer composed of six subunits. Each subunit contains one acidic polypeptide and one basic polypeptide linked by disulfide bond (S-S).

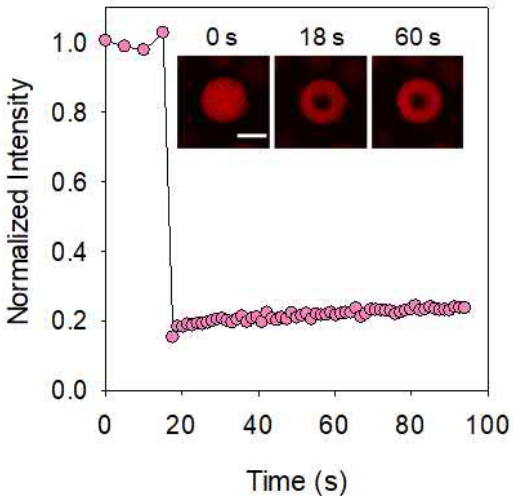

Figure S2. Negligible fluorescence recovery during FRAP measurement of a coacervate droplet indicates high viscosity of the coacervate. The inserts show the coacervate droplet (false colored) before and after photo bleaching at different time points. The scale bar represents 5 μm. Protein coacervates were prepared by mixing equal volume of protein solution (5 g/L) with 0.2 M NaCl solution, giving a final protein concentration of 2.5 g/L containing 10% FITC-labeled protein and NaCl concentration of 0.1 M at 23 °C. The protein solution was prepared from a stock solution of 20 g/L at pH 7.4.

G1
TDEQQQRPQEEEEEEEEDEKPQCKGKDKHCQRPRGSQSK
G2
MRKPQQEEDDDDEEEQPQCVETDKGCQRQSK
G3
TEEQQQRPEEEEKPDCDEKDKHQSQ
G4
WQEQQDEDEDEDEDDEDEQIPSHPPRRPSHGKREQDEDEDEDEDKPRPSRSQGKREQDQDQDEDE
DEDEDQPRKSREWRSKKTQPRRPRQEEPRERG
G5
WQEQEDEDEDEDEEYGRTPSYPPRRPSHGKHEDDEDEDEEEDQPRPDHPPQRPSRPEQQEPRGRG

Figure S3. Sequence of the hypervariable region (HVR) of the carboxyl ends of the acidic polypeptides of glycinin subunits (G1-G5, encoded by the five respective glycinin genes) with acidic (anionic) residues colored red, basic (cationic) residues colored purple, polar residues colored green and non-polar residues colored black.[8]

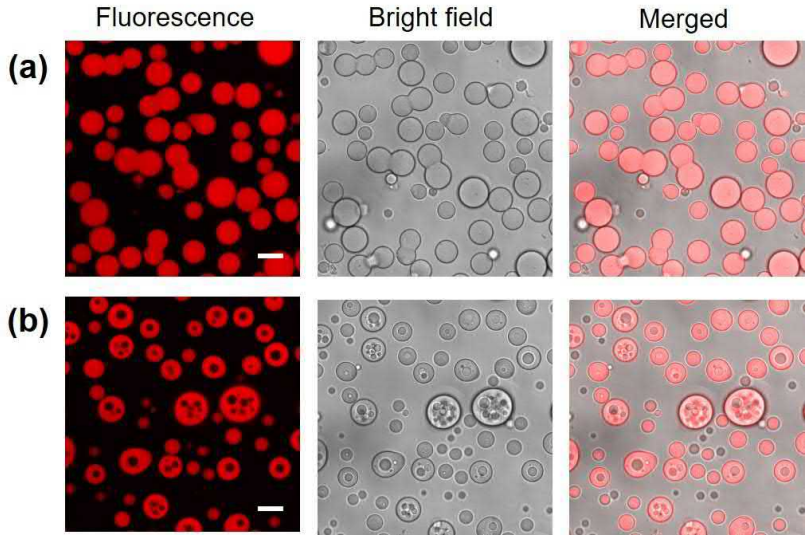

Figure S4. Fluorescence, bright-filed and the corresponding merged images of soy glycinin coacervates (a) and hollow condensates (b). The fluorescent dye rhodamine B preferentially partitions in the protein-dense phase. (a) Protein coacervates were prepared by mixing soy glycinin solution (20 g/L, pH 7.4) with equal volume of 0.2 M NaCl solution at 23 ºC to yield a protein suspension with protein concentration of 10 g/L and NaCl concentration of 0.1 M. The suspension was mixed with rhodamine B (5 mg/L) to stain the coacervates. (b) NaCl concentration of the coacervates suspension in (a) was increased from 0.1 to 0.175 M by mixing with equal volume of 0.25 M NaCl to produce hollow condensates. The scale bars are 20 μm.

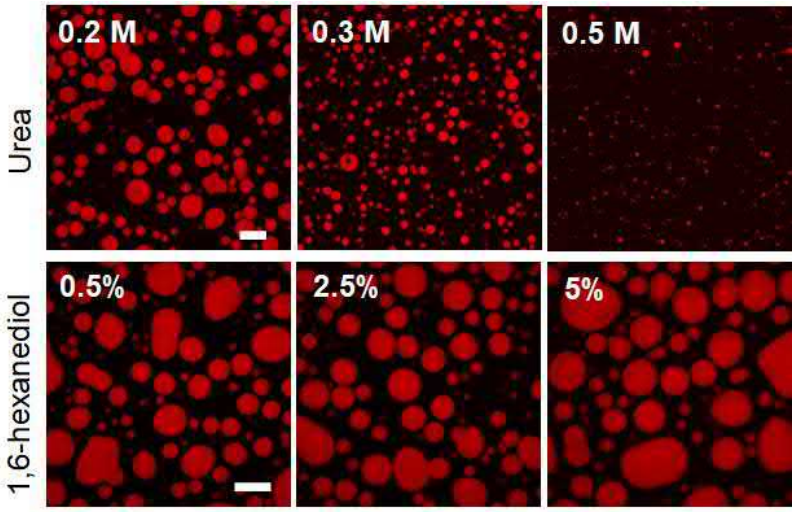

Figure S5. Influence of urea and 1,6-hexanediol on coacervation. Soy glycinin solution (20 g/L, pH 7.4) was mixed with equal volume of 0.2 M NaCl solution containing different concentration of urea (0.4-1 M) or 1,6-hexanediol (1-10 wt%) at 23 ℃ to yield respectively urea concentration of 0.2-0.5 M or 1,6-hexanediol concentration of 0.5-5 wt%. Rhodamine B (5 mg/L) was used to stain the protein coacervates. Images were taken immediately after sample preparation (~30 sec). The scale bars represent 20 μm.

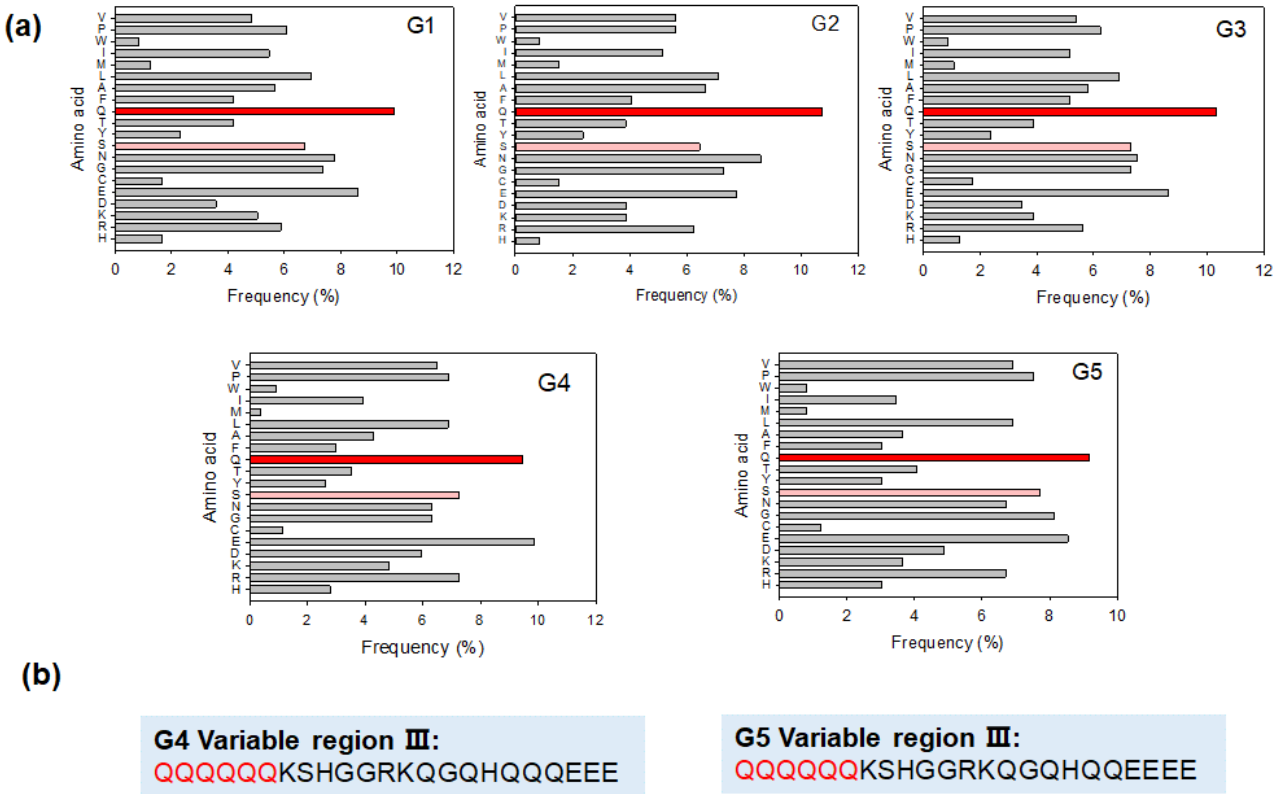

Figure S6. (a) Amino acid composition of glycinin subunits encoded by the five respective glycinin genes.[8] The frequency of glutamine (Q) and serine (S) were colored red and pink, respectively. (b) Sequence of the variable region III of G4 and G5 encoded by the glycinin genes with polyglutamine sequence highlighted in red.[9]

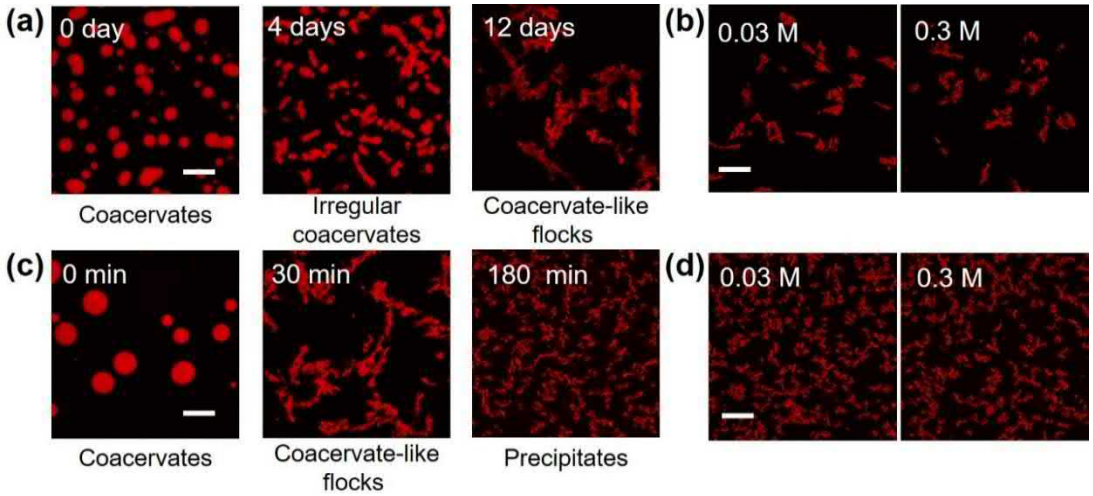

Figure S7. Influence of molecular restructuring on the protein ability to undergo coacervation. (a) Soy glycinin (5 g/L) was kept in salt free solution for different periods at 4 ºC as indicated on the images. After this period, the solution was mixed with an equal volume of 0.2 M NaCl to reach $C^{\triangle}$ and observed with CLSM using rhodamine B (5 mg/L). (b) The salt concentration of the suspension made from glycinin solution that has aged for 12 days in panel (a) was adjusted out of the coacervation region R2 to 0.03 or 0.3 M NaCl. No changes of the flocks were observed indicating high stability of the protein aggregate. (c) Soy glycinin (10 g/L) was mixed with 20 mM DTT and kept stirring at 23 ºC for different time as indicated on the images and subsequently mixed with equal volume of 0.2 M NaCl to reach $C^{\triangle}$ prior to imaging. (d) NaCl concentration of the suspension made from glycinin solution incubated with DTT for 180 min in panel (c) was adjusted out of the coacervation region R2 to 0.03 or 0.3 M NaCl. The scale bars represent 20 μm.

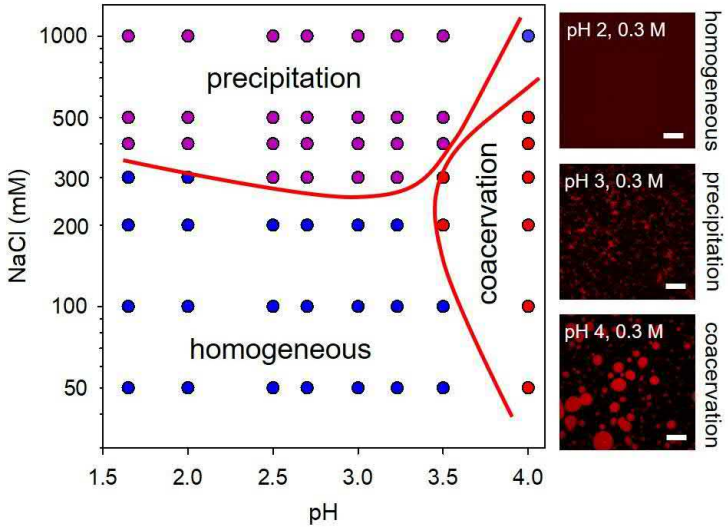

Figure S8. Influence of pH on the phase behavior of glycinin when it is positively charged. Soy glycinin solution (20 g/L) was adjusted to different pH below the isoelectric point (~pH 5.1). The protein suspension was mixed with equal volume of NaCl solution and the microstructure of the suspension was observed under the microscope to determine the conditions where the coacervation occurred. The red, purple and blue solid circles represent observed coacervation, precipitation and homogeneous solution, respectively, with representative images on the right observed by CLSM. The red lines are guides to the eye. The observation of precipitation was due to the denaturation of glycinin at acidic conditions.[10] The scale bars represents 20 μm.

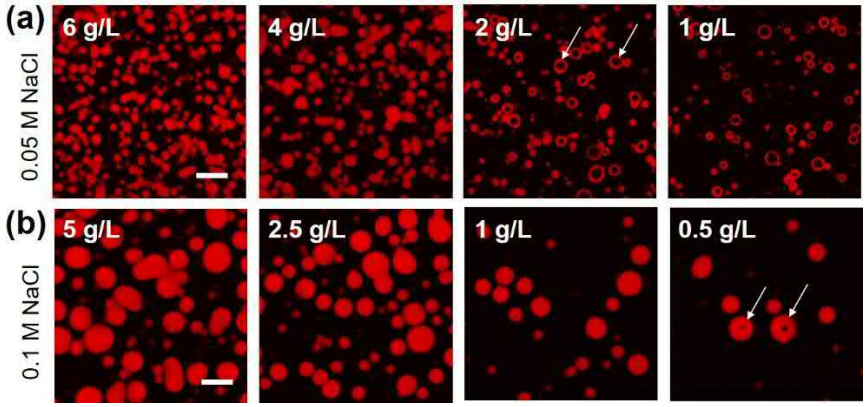

Figure S9. Decreasing protein concentration by dilution leads to cavity formation. Protein coacervates were prepared by mixing soy glycinin solution (20 g/L, pH 7.4) with equal volume of 0.1 or 0.2 M NaCl solution at 23 ºC to yield a protein suspension with soy glycinin concentration of 10 g/L and NaCl concentration of 0.05 or 0.1 M; 0.05 M is closer to the lower phase boundary (C^*) compared to 0.1 M. The protein concentration of the coacervate suspensions were then decreased by diluting with 0.1 M or 0.05 M NaCl solution, keeping the salt concentration fixed and the corresponding microstructures of the suspension was probed by CLSM using rhodamine B (5 mg/L). (a) Microstructure change of coacervates prepared at 0.05 M NaCl upon dilution. (b) Microstructure change of coacervates prepared at 0.1 M NaCl upon dilution. Arrows point to cavities formed inside the protein-rich droplets. The scale bars represent 20 μm.

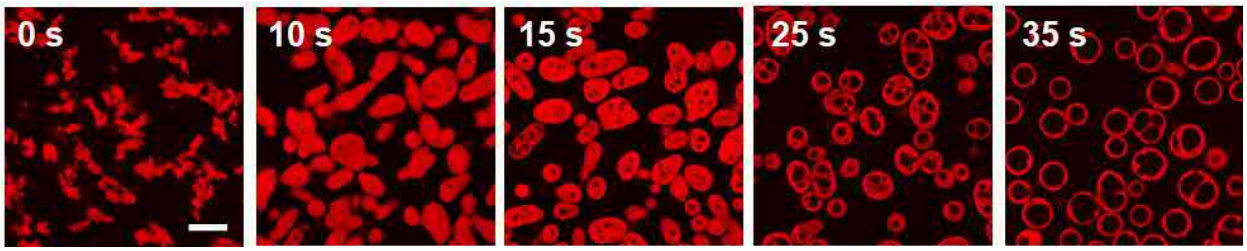

Figure S10. Transition from non-spherical coacervates to spherical domains during cavity formation. Protein coacervates were prepared by mixing soy glycinin solution (20 g/L, pH 7.4) with equal volume of 0.1 M NaCl solution at 23 ºC to yield a protein suspension with protein concentration of 10 g/L and NaCl concentration of 0.05 M. After glycinin and salt solution were mixed, the protein suspension (1 mL) in a vial was immediately transferred into a water bath at 40 ºC shaking by hand. At different time point as indicated in the images, the microstructure of the sample was imaged by CLSM using rhodamine B (5 mg/L) within 1 min after the suspension was placed into the observation chamber. The scale bar represents 20 μm.

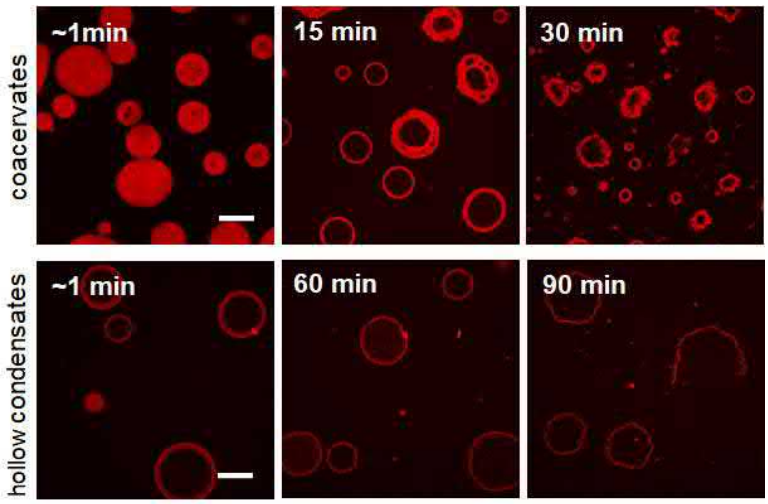

Figure S11. Influence of urea on the stability of coacervates and hollow condensates. To form coacervates, soy glycinin solution (20 g/L, pH 7.4) was mixed with equal volume of 0.2 M NaCl solution. Hollow condensates were produced by mixing the coacervates suspension with equal volume of 0.35 M NaCl solution. The coacervate and hollow condensate suspension were then mixed with equal volume of 0.1 M NaCl containing 0.2 M urea and 0.225 M NaCl solution containing 0.8 M urea, respectively at 23 ºC to yield a protein suspension with urea concentration of 0.1 M for coacervates and 0.4 M for hollow condensates (below the respective concentrations, coacervates and hollow condensates appeared stable for at least half an hour). Rhodamine B (5 mg/L) was used to stain the protein dense phase. Images were taken at different incubation time as indicated on the images. The scale bars represent 20 μm.

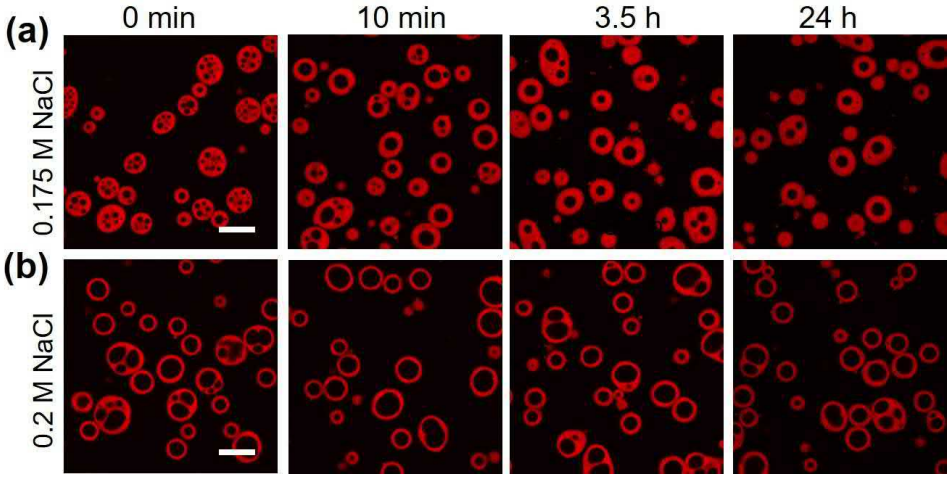

Figure S12. The morphology of hollow condensates is preserved over time. The hollow condensates were formed by mixing equal volume of coacervate suspension (pH 6.85, 0.1 M NaCl) with 0.25 or 0.3 M NaCl giving a final salt concentration of 0.175 M (a) or 0.2 M (b) at a final protein concentration of 5 g/L. The mixtures were observed under the microscope using rhodamine B (5 mg/L) at different time points as indicated above the images. The scale bars represent 20 μm.

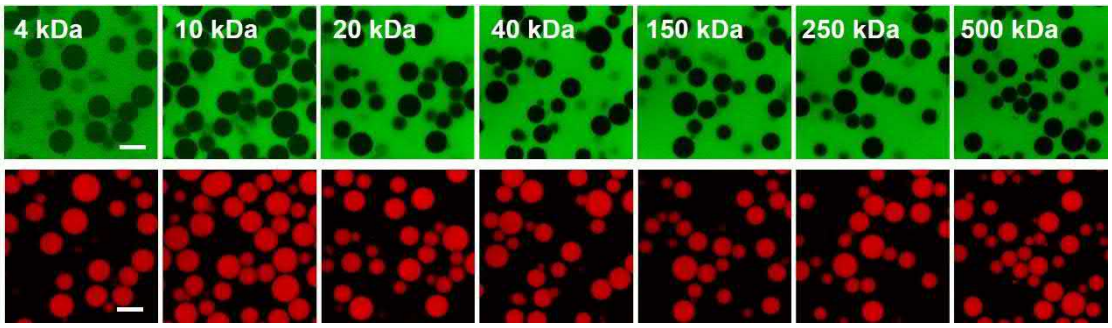

Figure S13. CLSM images of protein coacervates incubated with dextran of various M_w (indicated on the upper images). Protein coacervates were prepared by mixing soy glycinin solution (20 g/L, pH 7.4) with equal volume of 0.2 M NaCl solution at 23 ºC to yield a protein suspension with protein concentration of 10 g/L and NaCl concentration of 0.1 M. The coacervate suspension was then mixed with FITC-dextran (1 mg/mL) and rhodamine B (5 mg/L). The green fluorescence signal represents FITC-dextran. The red signal represents rhodamine B, which stains the coacervates. The scale bars represent 40 μm.

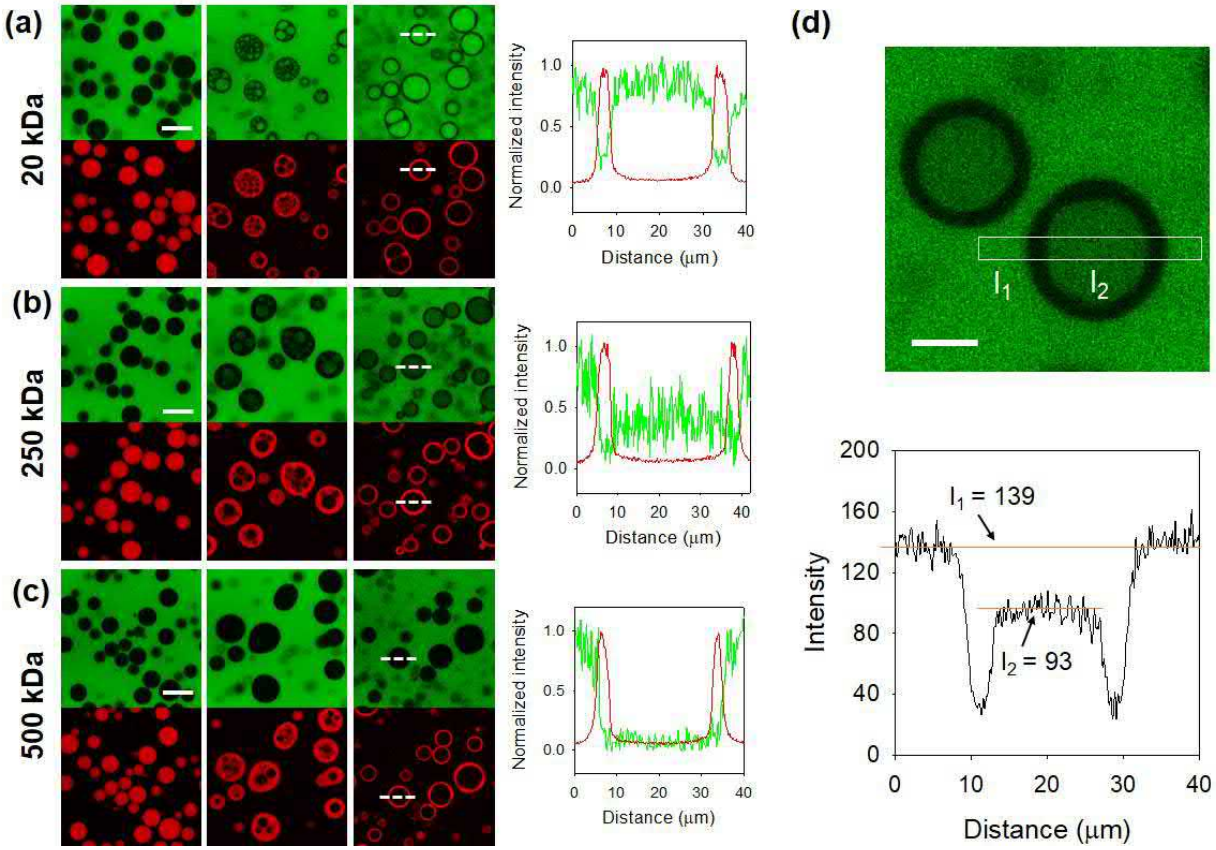

Figure S14. Partitioning of dextran into hollow condensates. The ionic strength was increased from 0.1 to 0.225 M to trigger cavity formation in coacervates mixed with FITC-dextran as shown in Figure S13. (a-c) Confocal cross-section images before (left images), during (middle) and 5 min after (right) cavity formation were taken. The green fluorescence signal represents FITC-dextran. The red signal represents rhodamine B (5 mg/L), which stains the protein-dense phase. The corresponding intensity profiles were measured 5 min after cavity formation along a horizontal

line (dashed line in the images) passing through the center of individual hollow condensates. (a) Dextran 20 kDa permeates into the formed cavity and is excluded from the cavity wall. (b) Dextran 250 kDa partially permeates into the formed cavity and is excluded from the cavity wall. (c) Dextran 500 kDa does not permeate through the wall of the hollow condensate. The scale bars represent 40 μm. (d) Measuring the permeation coefficient of FITC-labeled dextran with different molecular weight as assessed from fluorescence signal distribution. A rectangular bar was drawn across the center of the hollow condensates and the average intensities in the bulk solution (I_1) and that in the cavity (I_2) were analyzed by Image J. The permeation coefficient was calculated as the ratio I_2/ I_1. The scale bar is 10 μm.

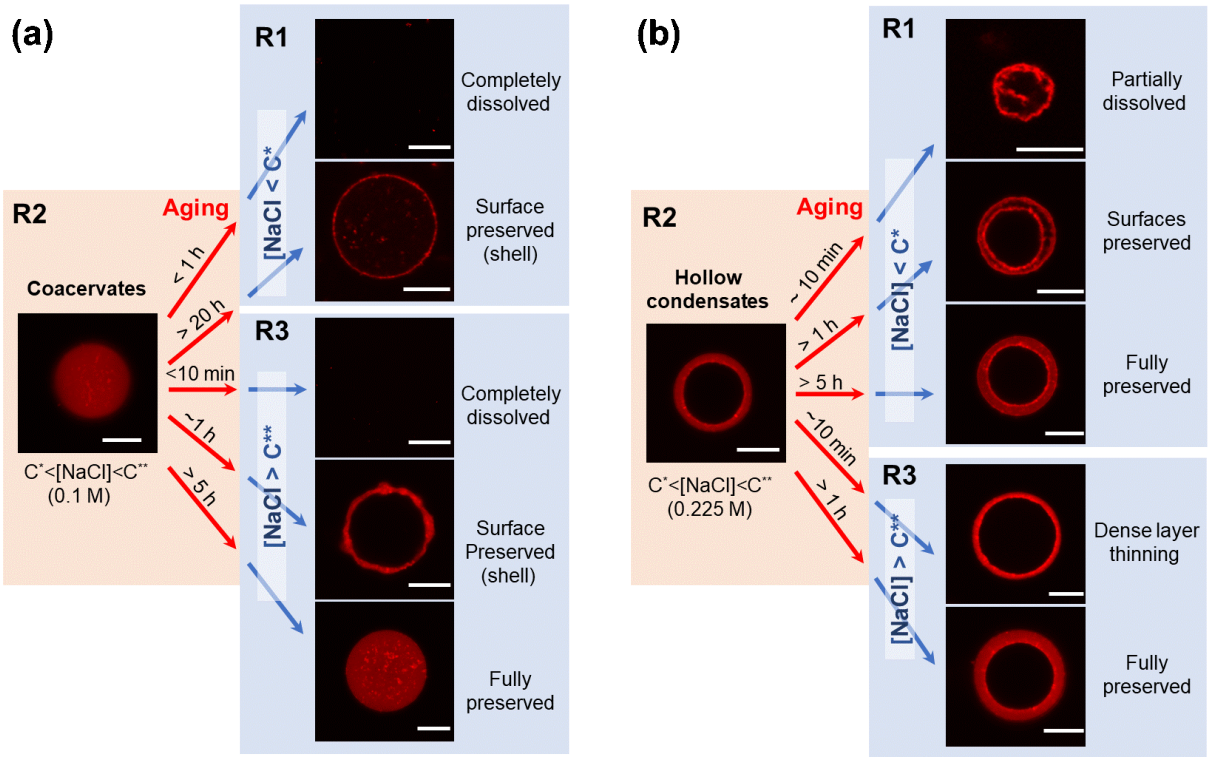

Figure S15. Influence of aging on the stability of soy glycinin coacervates (a) and hollow condensates (b) upon shifting from region R2 of phase separation to regions of homogeneity R1/R3. The coacervate suspension was prepared by mixing protein solution (pH 7.4, 20 g/L) with equal volume of 0.2 M NaCl solution at 23 ºC, yielding a final salt concentration of 0.1 M which falls in coacervation region R2, i.e. $C^*<[NaCl]<C^{**}$(see Figure 1 in the main text). The hollow condensate suspension was prepared by mixing the coacervate suspension with an equal volume of 0.35 M NaCl solution, yielding a final salt concentration of 0.225 M which is still in region R2. The two suspensions (coacervates and hollow condensates) were then aged at 23 ºC under mild stirring for different time. At different time points (the duration of aging is indicated above the red arrows), the suspensions were mixed with water to shift [NaCl] to 0.03 M which falls in homogeneity region R1, i.e. $[NaCl]< C^*$ or with equal volume of NaCl solution to shift [NaCl] to 0.3 M which falls in homogeneity region R3, i.e. $[NaCl]> C^{**}$. Microstructures of the dense phase were imaged by CLSM using rhodamine B (5 mg/L). The scale bars represent 10 μm.

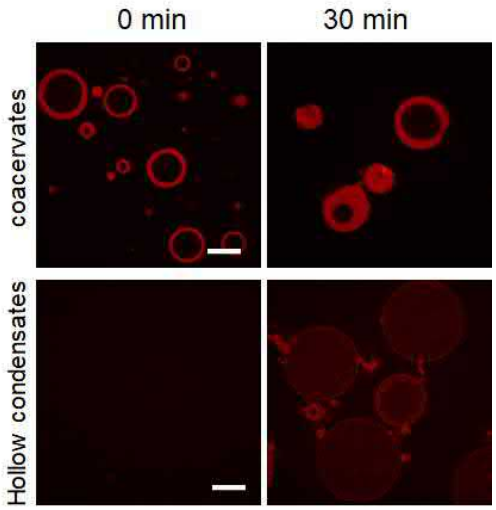

Figure S16. Aging strengthens the hydrophobic interaction. To form coacervates, soy glycinin solution (20 g/L, pH 7.4) was mixed with equal volume of 0.2 M NaCl solution. Hollow condensates were produced by mixing the coacervate suspension with equal volume of 0.35 M NaCl solution. After aging at 23 °C for 0 and 30 min as indicated above the images, the coacervate and hollow condensate suspensions were respectively mixed with equal volume 0.1 M NaCl containing 0.8 M urea and 0.225 M NaCl solution containing 1.6 M urea at 23 ºC to yield a protein suspension with urea concentration of 0.4 M for the coacervates and 0.8 M for the hollow condensates. Rhodamine B (5 mg/L) was used to stain the protein-dense phase. The scale bars represent 20 μm. In the presence of 0.4 M urea, the coacervates transformed into hollow condensates immediately. When aged for 30 min, the dense phase was largely preserved upon urea addition. In the presence of 0.8 M urea, the hollow condensates dissociated immediately. When aged for 30 min, the structure was partially preserved.

Supplementary movies

Movie 1. Coalescence dynamics of protein coacervates. Soy glycinin solution (5 g/L, pH 7.5) was mixed with equal volume of NaCl solution (0.2 M). Then, a suspension of 20 μL was transferred (within 30 s) into the observation chamber with BSA coated coverslip and immediately imaged. Time-lapse images were captured at an interval of 1.05 seconds with a frame rate of 40 fps (frames per second) in the movie. The duration of the movie in real time is ~12.5 min. Time zero corresponds to ~30 s during which the suspension was mixed and transferred to the observation chamber.

Movie 2. Transition from coacervates to hollow condensates by increasing ionic strength. Soy glycinin solution (20 g/L, pH 7.4) was mixed with an equal volume of NaCl solution (0.2 M). The phase transition was subsequently triggered by changing [NaCl] to 0.175 M by carefully diluting the protein suspension with equal volume of 0.25 M NaCl solution on the coverslip. The protein was stained with rhodamine B. Time-lapse images of the cross section of coacervates were captured at an interval of 1.29 s with a frame rate of 10 fps in the movie. The duration of the movie in real time is ~172 s. Time zero corresponds to 30 s after the suspension was mixed with salt. The scale bar is 10 μm.

Movie 3. Transition from coacervates to hollow condensates induced by increasing pH. Soy glycinin solution (20 g/L, pH 7.4) was mixed with equal volume of NaCl solution (0.2 M). The phase transition was subsequently triggered by increasing [NaOH] to 0.5 mM by carefully diluting the protein suspension with equal volume of 1 mM NaOH solution on the coverslip. The protein was stained with rhodamine B. Time-lapse images of cross sections of coacervates were captured at an interval of 2 seconds with a frame rate of 50 fps in the movie. The duration of the movie in real time is 10 min. Time zero corresponds to 30 s after the suspension was mixed with the NaOH solution. The scale bar is 10 μm.

Movie 4. Transition from coacervates to hollow condensates by increasing temperature. Soy glycinin solution (20 g/L, pH 7.4) was mixed with equal volume of NaCl solution (0.2 M). Suspensions of 20 μL was deposited to the observation chamber which had been warmed up to 40 ºC by microscope heating insert. The temperature of the observation chamber in the heating insert was measured by an infrared thermometer. The protein was stained with rhodamine B. Time-lapse images of the cross section of the coacervates were captured at an interval of 5 seconds with a frame rate of 50 fps in the movie. The duration of the movie in real time is 30 min. Time zero corresponds to 1 min after the suspension was transferred to the observation chamber. The scale bar is 10 μm.

References

(1) Nagano, T.; Hirotsuka, M.; Mori, H.; Kohyama, K.; Nishinari, K. Dynamic viscoelastic study on the gelation of 7S globulin from soybeans. *J. Agric. Food Chem.* **1992,** *40*, 941−944.

(2) Brangwynne, C. P.; Mitchison, T. J.; Hyman, A. A. Active liquid-like behavior of nucleoli determines their size and shape in Xenopus laevis oocytes. *Proc. Natl. Acad. Sci. U. S. A.* **2011,** *108* (11), 4334−4339.

(3) Eggers, J.; Lister, J. R.; Stone, H. A. Coalescence of liquid drops. *J. Fluid Mech.* **1999,** *401*, 293−310.

(4) Aarts, D. G. A. L.; Schmidt, M.; Lekkerkerker, H. N. W. Direct visual observation of thermal capillary waves. *Science* **2004,** *304,* (5672), 847.

(5) Badley, A. R.; Atkinson, D.; Hauser, H.; Oldani, D.; Green, J. P.; Stubbs, J. M. The structure, physical and chemical properteis of soy bean protein glycinin. *Biochim. Biophys. Acta, Protein Struct.* **1975,** *412,* 214−228.

(6) Sokolova, A.; Kealley, C. S.; Hanley, T.; Rekas, A.; Gilbert, E. P. Small-angle X-ray scattering study of the effect of pH and salts on 11S soy glycinin in the freeze-dried powder and solution states. *J. Agric. Food Chem.* **2010,** *58* (2), 967−974.

(7) Sağlam, D.; Venema, P.; de Vries, R.; van der Linden, E. The influence of pH and ionic strength on the swelling of dense protein particles. *Soft Matter* **2013,** *9* (18), 4598–4606.

(8) Nielsen, N. C.; Dickinson, C. D.; Cho, T.-J.; Thanh, V. H.; Scallon, B. J.; Fischer, R. L.; Sims, T. L.; Drews, C. N.; Goldberg, R. B. Characterization of the glycinin gene family in soybean. *Plant Cell* **1989,** *1*, 313−328.

(9) Withana-Gamage, T. S.; Wanasundara, J. P. D. Molecular modelling for investigating structure–function relationships of soy glycinin. *Trends Food Sci. Technol.* **2012,** *28* (2), 153−167.

(10) Lakemond, C. M. M.; de Jongh, H. H. J.; Hessing, M.; Gruppen, H.; Voragen, A. G. J. Soy glycinin: Influence of pH and ionic strength on solubility and molecular structure at ambient temperatures. *J. Agric. Food Chem* **2000,** *48*, 1985−1990.